

# Anti-UAV: A Large Multi-Modal Benchmark for UAV Tracking

Nan Jiang<sup>†</sup>, Kuiran Wang<sup>†</sup>, Xiaoke Peng<sup>†</sup>, Xuehui Yu, Qiang Wang, Junliang Xing, Guorong Li, Guodong Guo, Jian Zhao<sup>‡</sup> and Zhenjun Han<sup>‡</sup>

**Abstract**—Unmanned Aerial Vehicle (UAV) offers lots of applications in both commerce and recreation. With this, monitoring the operation status of UAVs is crucially important. In this work, we consider the task of tracking UAVs, providing rich information such as location and trajectory. To facilitate research in this topic, we propose a dataset, Anti-UAV, with more than 300 video pairs containing over 580k manually annotated bounding boxes. The releasing of such a large-scale dataset could be a useful initial step in research of tracking UAVs. Furthermore, the advancement of addressing research challenges in Anti-UAV can help the design of anti-UAV systems, leading to better surveillance of UAVs. Besides, a novel approach named dual-flow semantic consistency (DFSC) is proposed for UAV tracking. Modulated by the semantic flow across video sequences, the tracker learns more robust class-level semantic information and obtains more discriminative instance-level features. Experimental results demonstrate that Anti-UAV is very challenging, and the proposed method can effectively improve the tracker’s performance. The Anti-UAV benchmark and the code of the proposed approach will be publicly available at <https://github.com/ucas-vg/Anti-UAV>.

**Index Terms**—unmanned aerial vehicle, single object tracking, deep tracking, multi-modal.

## I. INTRODUCTION

Object tracking is to locate an object across a series of video frames [1–3]. It is widely used in video surveillance [4], maritime rescue [5][6], biology robotics [7], and self-driving cars [8][9]. Recently, the accessibility and popularity of Unmanned Aerial Vehicle (UAV) for commercial and recreational use have significantly surged. It has a wide range of applications, such as autonomously landing [10], target tracking and following [11]. Behind these practical applications, it is crucial to monitor the operation status of

UAV, including locations and trajectory. To this end, this article focuses on tracking UAV.

In literature, most of object trackers are based on RGB information [12–16]. However, when in the poor light conditions, these trackers might not be able to find useful cues, leading to unreliable results. To alleviate this, some works consider using infrared (IR) images for object tracking [17][18]. The crucial drawback of infrared images is that it usually has a low resolution, providing inadequate information for trackers. Based on the above analysis, we think it is important to fuse information from visible RGB and IR images for tracking UAVs. Specifically, leveraging multi-modal information is beneficial for learning accurate and robust UAV trackers [19][20]. For this purpose, a multi-modal dataset is required to study the task of tracking UAV.

To the best knowledge, there is no multi-modal UAV tracking benchmark for UAV. In the community, the tracking datasets mainly contains general objects (*e.g.*, car and person). To mitigate this, we introduce a new dataset, Anti-UAV, to facilitate the research on UAV tracking. Anti-UAV contains high-quality and high-definition video sequences of both RGB and IR. Each sequence is annotated with bounding boxes, attributes, and flags indicating whether the target object exists. It is worth noting that RGB and IR video sequences are *paired* in Anti-UAV. Thus, the proposed dataset supports both single-modal and multi-modal UAV tracking.

Furthermore, based on the fact that Anti-UAV has only one category, this work propose a novel training strategy named dual-flow semantic consistency (DFSC), containing class-level semantic modulation (CSM) stage and instance-level semantic modulation (ISM) stage for UAV tracking. On the one hand, all different sequences share one trait: the labeled objects in them are only UAVs, which means the network can utilize the cross-sequence features. The tracker in the CSM stage adopts class-level semantic modulation to retrieve anchors that may contain UAV as far as possible to reduce the intraclass differences. On the other hand, the tracker pays more attention to the fine-grained instance-level features to distinguish between the real UAV instance of the current tracking sequence and the similar distractors in the ISM stage. Since the DFSC method only works in training, it will not affect the calculation and time consumption in the inference time.

The main contributions of this work can be summarized as:

- A multi-modal dataset named Anti-UAV, the first UAV tracking dataset, is constructed. The Anti-UAV dataset consists of 318 RGB-T video pairs with ground-truth in different scenes and environmental conditions, where

<sup>†</sup> Equal contribution.

<sup>‡</sup> These authors jointly supervised this work: Jian Zhao and Zhenjun Han.

N. Jiang, K. Wang, X. Peng, X. Yu, and Z. Han are with the School of Electronic, Electrical and Communication Engineering, University of Chinese Academic of Sciences (UCAS), Beijing, 101408 China. E-mail: {jiangnan18, wangkuiran19, pengxiaoke19, yuxuehui17}@mails.ucas.ac.cn, hanzhj@ucas.ac.cn.

Q. Wang and J. Xing is with the National Laboratory of Pattern Recognition, Institute of Automation, Chinese Academy of Sciences (CASIA), and also with the School of Artificial Intelligence, University of Chinese Academy of Sciences (UCAS), Beijing, China. E-mail: {qiang.wang, jlxing}@nlpr.ia.ac.cn.

G. Li is with the School of Computer and Control Engineering, University of Chinese Academy of Sciences (UCAS), Beijing, 101408, China, and also with the Key Laboratory of Big Data Mining and Knowledge Management, UCAS, Beijing, 101408, China. E-mail: liguorong@ucas.ac.cn.

G. Guo is with Institute of Deep Learning, Baidu Research and National Engineering Laboratory for Deep Learning Technology and Application. Email: guoguoandong01@baidu.com.

J. Zhao is with Institute of North Electronic Equipment, Beijing, China. Homepage: <https://zhaoj9014.github.io/>. E-mail: zhaojian90@u.nus.edu.

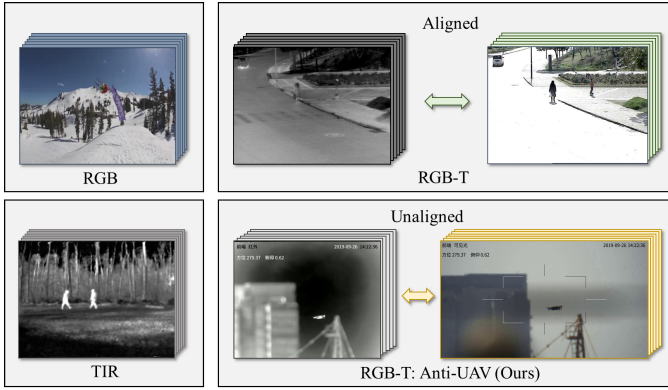


Fig. 1. Object tracking datasets. Visible images can provide more details, however, are susceptible to illumination. Whereas infrared images have an opposite problem. The Anti-UAV is a RGB-T dataset. However, unlike other RGB-T datasets, Anti-UAV is composed of unaligned video sequence pairs.

“RGB” and “T” represent visible light and thermal infrared respectively. It has been released to public for free in academic research.

- According to UAV tracking challenges, to better evaluate the tracker’s performance, a evaluation metric that focuses on judging the state of UAV is given. Experimental valuation and analysis of more than 40 trackers on Anti-UAV are provided for a series of baselines. Extensive experiments are provided to study the impact of different aspects of training data on deep trackers’ performance.
- A novel dual-flow semantic consistency (DFSC) training method is proposed to make the tracker obtains robust and representative feature after class-level and instance-level semantic modulation. The DSFC significantly outperforms the baselines.

Served as a large-scale multi-modal benchmark, Anti-UAV drives the future research on the frontiers of tracking UAVs in the wild. With the above innovations and contributions, we have organized the CVPR 2020 Workshop on the 1<sup>st</sup> Anti-UAV Challenge. These contributions together significantly benefit the community.

## II. RELATED WORK

In the following, an overview of the various researches on object tracking will be presented. The related tasks are grouped into the field into RGB tracking, TIR tracking, and RGB-T tracking, as shown in Fig. 1. Then the similarities and differences between some trackers and the method proposed in this paper are analyzed at length.

### A. Tracking Dataset

**RGB Tracking Dataset.** As given in Tab. I, there are several datasets for RGB object tracking. Among them, OTB [21][22], VOT [23–25], ALOV++ [2], and TC128 [26] are for single object tracking. In OTB and TC128, each frame of a video sequence is annotated with 11 different properties and vertical borders while 314 video sequences with 14 attributes make up ALOV++. VOT with 60 video sequences, introduces the

rotary bounding box, and studies the target tracking annotation extensively.

More recently, TrackingNet [33] and LaSOT [32] offer large-scale tracking datasets. TrackingNet selects about 30,000 videos to form the training subset from YouTube-BB [48]. As for the evaluation subset, it collects 511 videos whose category distribution is similar to the training subset. LaSOT collects and annotates 14,000 videos manually. GOT-10k [34] is a relatively large dataset, and covers a broader range of object categories. Compared with other benchmarks, GOT-10k is the only one following the one-shot evaluation protocol to avoid bias in evaluating the seen class.

**TIR Tracking Dataset.** As a dataset that simulates aerial TIR object tracking and detection, PDT-ATV [36] consists of 8 sequences captured from a low frame rate and low resolution TIR camera. Composed of 16 sequences of over 60K frames with high resolution, BU-TIV [37] is intended for various TIR visual tasks including tracking, group motion estimation and counting. LTIR [39] is the first standard TIR target tracking benchmark with 20 sequences, 6 target classes, and an evaluation toolkit. VOT-TIR16 [40], an extension of VOT-TIR15 [39], contains 25 sequences and 8 object classes, making it more challenging than VOT-TIR15. VOT-TIR16 has six challenging subsets used to evaluate specific attributes of the tracker. Lately, LSOTB-TIR [42], a large-scale and highly diverse TIR target tracking benchmark, is constructed. Containing 1400 TIR sequences over 600K frames, LSOTB-TIR includes an evaluation dataset and a training dataset.

**RGB-T Tracking Dataset.** Several RGB-T tracking datasets have been proposed. The OSU-CT dataset [43] contains 6 pairs of RGB-T video sequences, in which each pair of sequences came from two different locations. Most of videos in OSU-CT have limited size, low diversity and high prejudice. A large RGB-T dataset, RGBT210 [46], consists of 210 RGB-T video pairs recorded on a mobile platform, which enriches the diversity of the dataset. Li *et al.* collects a total of 234 video pairs to construct a large RGB-T tracking dataset named RGBT234 [47] including more challenging RGB-T video, baseline algorithms, attributes, and evaluation metrics.

Compared with the above datasets, it is worth noting that the video sequence pairs in Anti-UAV are not aligned, which is more challenging than other RGB-T datasets.

### B. Trackers

**RGB Based Trackers.** Most traditional trackers mainly base on filtering [49–55]. In the initialization stage, to effectively distinguish the background and target, a discriminative filter is trained based on the minimum mean square error of the output result according to the first frame sample. During tracking procedure, the filter finds the target’s position through the response image of the search area. The higher value of the response image is, the stronger correlation between the position’s image and the target is.

Despite some advantages of correlation filter in precision and efficiency, there are still some drawbacks. The performance of most existing trackers relies on an appropriate search area. Setting unreasonable search area will cause the situation

TABLE I

A COMPARISON OF ANTI-UAV WITH OTHER SINGLE OBJECT TRACKING (SOT) DATASET IN TERMS OF THE NUMBER OF VIDEO SEQUENCE, BOUNDING BOX, AND ATTRIBUTE. ANTI-UAV IS MUCH LARGER THAN MOST RGB-T TRACKING DATASET. IN THE MEANTIME, ANTI-UAV IS SPECIFICALLY FOR UAV TRACKING AND PROVIDES CORRESPONDING TRAINING SET.

Dataset	Total		Train		Test		Attribute	
	Sequences	Bboxes	Sequences	Bboxes	Sequences	Bboxes		
RGB	OTB2013 [21]	50	29.4k	-	-	50	29.4k	11
	OTB2015 [22]	100	59k	-	-	100	59k	11
	VOT2014 [23]	25	10k	-	-	25	10k	5
	VOT2017 [24]	60	21k	-	-	60	21k	5
	VOT2019 [25]	60	19.9k	-	-	60	19.9k	5
	ALOV++ [2]	314	16k	-	-	314	16k	14
	TC128 [26]	128	55k	-	-	128	55k	11
	NUS_PRO[27]	365	135k	-	-	365	135k	12
	TLP[28]	50	648k	-	-	50	648k	6
	OxUxA [29]	366	155k	-	-	366	155k	6
	UAV123[30]	123	113k	-	-	123	113k	12
	UAV20L[30]	20	59k	-	-	20	59k	12
	Nfs [31]	100	38k	-	-	100	38k	9
	LaSOT [32]	1.4k	3.3M	1.1k	2.8M	280	685k	14
TrackingNet [33]	31k	14M	30k	14M	511	226k	15	
GOT-10k [34]	10k	1.5M	9.3k	1.4M	420	56k	6	
TIR	OSU-T [35]	10	0.2k	-	-	10	0.2k	-
	PDT-ATV [36]	8	4k	-	-	8	4k	-
	BU-TIV [37]	16	60k	-	-	16	60k	-
	ASL-TID [36]	9	4.3k	-	-	9	4.3k	-
	TIV [37]	16	63k	-	-	16	63k	-
	Terravic Motion IR [38]	18	5.5k	-	-	18	5.5k	-
	LTIR [39]	20	11.2k	-	-	20	11.2k	5
	VOT-TIR16 [40]	25	14k	-	-	25	14k	10
	PTB-TIR [41]	60	30k	-	-	60	30k	9
	LSOTB-TIR [42]	1400	606k	1280	524k	120	82k	12
RGB-T	OSU-CT [43]	6	17k	-	-	6	17k	-
	LITIV [44]	9	6.3k	-	-	9	6.3k	-
	GTOT [45]	50	15.8k	-	-	50	15.8k	7
	RGBT210 [46]	210	210k	-	-	210	210k	12
	RGBT234 [47]	234	233.8k	-	-	234	233.8k	12
	<b>Anti-UAV (Ours)</b>	318	585.9k	160	294.4k	91	168.4k	7

of missing target or tracking drift. Simultaneously, the training samples of correlation filters are usually target-centered and obtained utilizing cyclic displacement. The limitations of negative samples will also limit the ability of the filter to distinguish the background.

With the development of deep learning, neural networks are introduced to the object tracking. The first attempt to apply deep learning to tracking task is made by Wang *et al.*, who also creatively proposes the deep target tracking framework [56] of offline training with online fine-tuning. Since then, the research on the deep tracker has been widely carried out. From the aspect of structure, these methods can be divided into the methods based on pre-training network combined with correlation filter [57–61], siamese-based network [12–15], convolutional neural network [52, 62–66], and so on.

**TIR Based Trackers.** Since deep learning method has achieved great success in visual tracking, some works begin to introduce convolutional neural network (CNN) to improve the performance of TIR tracker.

MCFT [67] integrates deep features of VGGNet and correlation filter into a TIR tracker. LMSCO [68] makes a combination of appearance features and motion features to construct a TIR target tracking. As a multi-level similarity model, MLSSNet [69] is proposed for robust TIR tracking under a Siamese Network. Based on particle filter framework

for TIR target tracking, a mask sparse representation deep appearance model [70] is proposed to replace the previous random sampling for searching useful candidates.

**RGB-T Based Trackers.** The thermal infrared sensors are increasingly popular. Accordingly, the number of RGB-T tracking datasets has increased. Motivated by this, more and more works devote their efforts to study target tracking specifically for RGB-T datasets.

Wu *et al.* [71] use the spliced image patch of RGB and heat source to represent each sample sparsely in the target template space. In order to make full use of information, the authors of [20] combines the minimal operational tracking results for RGB and thermal mode calculations of sparse representation coefficients. However, when dealing with incidental disturbances or failures from individual sources, since the contribution of the available spectrum is equal, these methods may limit tracking performance. A weighted sparse representation regularized graph [46] is proposed to learn a robust object representation through visible and infrared images. In addition, some methods based on deep learning [72] and correlation filter [73] have been proposed.

### C. Image-based Training Strategy

Some works are dedicated to explore the relationship between different instances in the same image. Through a large

number of experiments, it is proved that reasonably defining the labels of instances in the same image can effectively improve the model’s performance. Besides, to overcome the pictures’ internal limitations, some research works study and analyze the instances’ relationship among different images.

**Intra-image Training Strategy.** Reasonable use of all instances on a single image can effectively improve the performance of the tracker. SPM [74] proposes a Series-Parallel Matching framework based on SiamFC [12] to meet the demand for stronger discriminative power and robustness. During the Coarse Match stage, the tracker focuses on robustness to reduce the intraclass diversity for the same object. It is expected that the target object can be discovered even though it is undergoing tremendous change in representation. GlobalTrack [75] proposes cross query loss to enhance the discriminative power of tracker through searching a same image using different but co-exist queries. Notably, this training strategy is also very efficient because features are shared in the feature extraction part.

It is worth mentioning that the premise of this training strategy’s implementation is that the training images belong to the object detection dataset. Only when the training set is such a dataset there will be multiple target bounding box labels on a single image. In contrast, DFSC can be applied to the single object tracking dataset, which focuses on the cross sequence images. Different query-search image pairs are used to improve the robustness of the tracker in the CSM stage.

**Inter-image Training Strategy.** Even if the intra-image training strategy has achieved some achievements, it still has some limitations, since it only utilizes information of instances on a single image. Thus, some works begin to focus on cross-image instances. Copying and pasting over parts of an image or the whole image has been successfully utilized as a training strategy in image classification, object detection, and so on.

Because there are too few difficult cases such as occlusion in 2D human keypoints dataset, the authors of [76] proposes a data augmentation method including artificially creating occlusion (paste background block to cover some key points of human body) and artificially constructing ambiguous image. This occlusion augmentation method [77] is also validated on 3D human keypoint dataset, which achieves the state-of-the-art performance. In the classification task, Mixup [78] mixes two random samples in proportion. The results of classification are allocated in proportion. While Cutmix [79] is to cut out a part of the region. Instead of filling the region with zero, it randomly fills with the pixel values of other data in the training set. The classification results are allocated according to a certain proportion. Unlike the methods mentioned above, the proposed method does not copy and paste on the image level but the feature level.

The authors of [80] argues that the imbalance between the non semantic background and the semantic distractor in the training data further hinders the tracker learning. Therefore, in the training stage, the author introduces the existing detection datasets to enrich the positive sample data to improve the tracker’s generalization ability; then, the author enriches the hard negative sample data to improve the discriminative ability of the tracker.

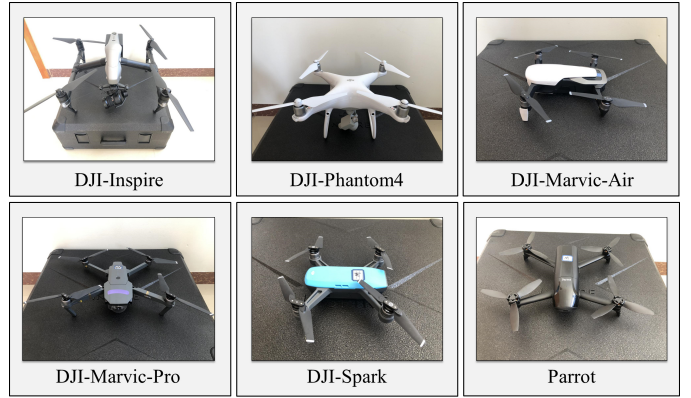


Fig. 2. Overview of UAVs for capturing multi-modal tracking data. In order to ensure the diversity of data, six types of UAVs, mainly from DJI and Parrot are utilized to collect tracking data.

As UAV is the only tracking category in Anti-UAV dataset, in the class-level semantic modulation (CSM), cross-sequence pairs are used to improve the robustness of the tracker which do not introduce an additional object detection training set. At the same time, it only operates in the current batch and shares the computation at the feature extraction stage.

### III. ANTI-UAV BENCHMARK

In this section, the details of Anti-UAV, including data collection, annotation, dataset statistics information, and evaluation protocols, are given as follows.

#### A. Data Collection

For the feasibility of tracking algorithms’ performance evaluation on large-scale Anti-UAV, 318 RGB-T video pairs are collected, each containing an RGB video and a thermal video, forming a large-scale dataset for discovering and tracking UAVs in the wild.

At present, the lack of large-scale UAV datasets makes it challenging to study detection and tracking algorithms. If a small-scale annotated UAV dataset is directly used for detection or tracking, a serious missing detection phenomenon will happen to the pre-trained tracker. As a result, the construction of a new large-scale UAV dataset is essential for the research of UAV tracking algorithms. We record several videos of various types of UAVs flying in the air. These videos include two lighting conditions (day and night), two light modes (infrared and visible) and diverse backgrounds (buildings, sky, cloud and trees *etc.*). Each video is stored in infrared and visible light modes in an MP4 file with a frame rate of 25FPS.

The following difficulties were encountered during the UAV data collection process:

- In flight, the wind speed will have a certain impact on the control of the UAV.
- The location of photoelectric tracking equipment is fixed with a limited field of vision.
- The uncoordinated cooperation between collector and pilot may lead to the loss of UAV in the field of acquisition.

- The UAV has limited endurance time and needs to be powered up after a short flight, resulting in a decrease in acquisition efficiency.

As for the types of UAVs, the following six types are adopted as shown in Fig. 2, which mainly from DJI and Parrot, including large UAV (DJI-Inspire), medium UAV (Dji-Phantom4), and small UAV (DJI-Marvic-Air, DJI-Marvic-Pro, DJI-Spark, Parrot).

### B. Annotation

To guarantee the annotation quality of the Anti-UAV dataset, a progressive strategy is adopted to accurately annotate the bounding box of UAV from coarse to fine. There are three stages in the process of data annotation.

**Coarse Annotation.** In the first stage, the data is coarsely annotated: (i) We annotate the attributes/scenes of each video, such as the size of UAV targets (large, medium and small), light condition (day or night), light mode (infrared or visible), the condition of occlusions (cloud, building, jungle) and possible false target (birds and civil aviation *etc.*). (ii) Each video is annotated every 25 frames. The annotation rules of this stage are as follows: If the target appears in the current frame, the flag is set as “1” and vice versa; the UAV is labeled with a rectangle that is close to the target. In the annotation files, the keyword “*exist*” can be “1” (True) or “0” (False), and the keyword “*get\_rect*” can be expressed as “[x1, y1, x2, y2]” (the coordinates of the upper left and lower right corner of the bounding box).

**Fine Annotation.** In the second stage, a round of selection is carried out on coarse annotated data results. According to the complexity, the videos are ranked in each scene. Then the top 10 are chosen for further annotation. After selection, there are 30 infrared videos and 30 visible videos left. Based on the results of coarse annotation, each video frame is annotated in detail and the annotation rules are the same with last stage.

**Inspection and Correction.** After the second stage, there are still some annotating errors such as bounding boxes with the over-large size and mislabeling of the frames with no target or a large occlusion area as “1”. Besides, visible video sequences taken at night may contain extremely blurred and distorted frames due to the pan-tilt’s fast-moving. In above cases, the annotations need to be removed. At last, the annotated videos are divided into sequences every 1000 frames.

### C. Dataset Details

**Dataset Splitting.** The Anti-UAV dataset is divided into training set, validation set, and test set. The training set and the validation set may come from non-overlapped clips of the same video, but the test set is entirely independent. Besides, the test set is much more complicated than the validation set. Anti-UAV has 318 video sequence pairs. Each pair consists of one RGB video and one infrared video. In all these video sequence pairs, 160 are divided into training set, 91 are assigned to test set, and the rest are used as validation set.

**Position Distribution.** As shown in Fig. 3, the positions of the boxes are mostly concentrated in the central area of the picture, and the larger transverse variance means that the horizontal

TABLE II  
ILLUSTRATION OF ATTRIBUTE ANNOTATION IN ANTI-UAV.

Attribute	Description
OV	Out-of-View the target leaves the view.
OC	Occlusion - the target object is partially occluded or heavily occluded.
FM	Fast Motion the ground-truth’s motion between two adjacent frames is larger than 60 pixels.
SV	Scale Variation the ratio of the bounding boxes of the first frame and the current frame is out of the range [0.66, 1.5].
LI	Low Illumination - the illumination in the target region is low.
TC	Thermal Crossover - the target has a similar temperature with other objects or background surroundings.
LR	Low Resolution the number of pixels inside the ground-truth bounding box is less than 400 pixels.

movements of UAV are in the majority. Besides, the range of motion of the target in the test set is more diverse. The test set’s fluctuation is larger than that of the training set in the horizontal and vertical directions.

**Scale Distribution.** The target size of UAV fluctuates widely in the whole Anti-UAV dataset. The scale distribution of UAV is given in Fig. 4 for better analysis. The size of the UAV object can be calculated as  $s(w, h) = \sqrt{w \times h}$ . The figure shows that the scale distribution of training set, the validation set, and the test set are all relatively similar. To a certain extent, the scale distribution of the test set looks more centralized and sharper. The average values of the target size of three sets are all less than 40 pixels.

### D. Attributes

The overall performance on Anti-UAV can not reflect the detailed difference of different trackers. To better measure the performance on a subset of the video with specific attributes, such as occlusion, binary attribute annotations is provided. In this condition, the evaluation metric helps identify the pros and cons of Anti-UAV trackers. Each video is annotated with the list of properties defined in Tab. II.

Seven attributes are provided for Anti-UAV, each of which is shown in Fig. 5. For better presenting the Anti-UAV, statistics are done for the specific situation of each attribute as shown in Fig. 6. According to the statistical results, the following conclusions can be reached:

- The proportion of target moving out of the view is relatively larger in the test set. But in absolute terms, this proportion is not high on the whole.
- The case that the target among adjacent frames moves more than 60 pixels takes up a large proportion in Anti-UAV, which is one of difficulties in UAV tracking.
- If the SV standard of OTB is followed, almost no sequence will be considered as SV. Since the scale changes rarely exceed [0.5, 2] in Anti-UAV, therefore, [0.66, 1.5] may be more suitable for UAV tracking.
- According to the video shooting division of day and night, the illumination degree of a visible light video sequence may affect multi-modal fusion. There are many video sequences shot in the day. A large number of videos shot at night also affect the UAV tracking of visible light

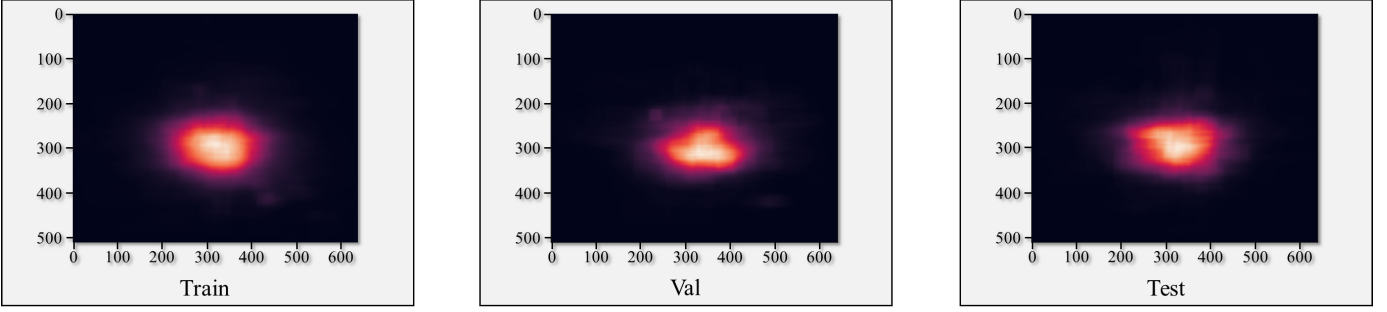


Fig. 3. UAV’s position distribution of sequences in each part of Anti-UAV. The locations of boxes are mainly concentrated near the center of the picture. Compared with vertical motions, the horizontal movements of UAV are more, which can be seen from variances in horizontal and vertical directions.

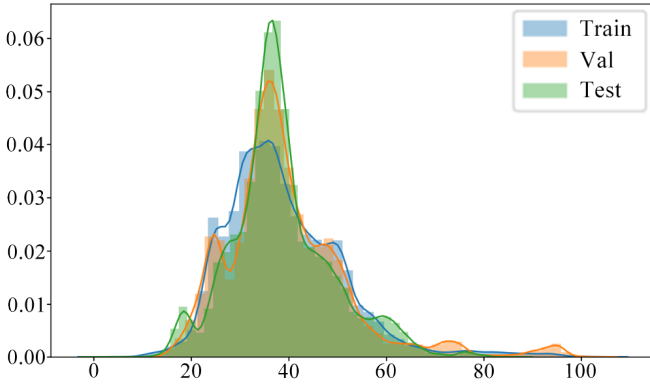


Fig. 4. Scale distribution of sequences in each part of Anti-UAV. The abscissa is UAV object’s size which can be calculated as  $s(w, h) = \sqrt{w \times h}$ .

sequences. At this time, it is necessary to make full use of the advantages of infrared sensors.

- According to the experimental results, the thermal crossover is the most intractable problem to solve. If a building or cloud appears in the background of the video sequence or a very similar false target appears, it is hard to tell them from the target in the infrared videos. At this time, it is necessary to use visible light sequence texture information to distinguish.

Attribute TC accounts for a large proportion of the whole Anti-UAV dataset. Therefore, it is necessary to partition the attribute TC more finely. Hence, the division of attribute TC is shown in Fig. 7, according to the tracking difficulty of the infrared video sequence.

### E. Evaluation Metrics

Professional annotators annotate all data with bounding boxes, attributes and flags indicating whether the target exists or not in each frame. Box coordinates are floats measured from the top left image corner. Moreover, an empty bounding box list denotes a “not exist” flag. In the tracking process, the tracker needs to obtain the tight bounding box of the UAV and perception of UAV status. In this case, the presence of UAV in the visual range is introduced into the evaluation metric:

$$SA = \sum_t \frac{IOU_t \times \delta(v_t > 0) + p_t \times (1 - \delta(v_t > 0))}{T}. \quad (1)$$

The  $IoU_t$  is Intersection over Union (IoU) between each tracking bounding box and corresponding ground-truth. The  $v$  are the ground-truth visibility flags (the tracker’s predicted  $p$  are used to measure the state accuracy). The state accuracy  $SA$  is averaged over all frames in a video sequence. The average state accuracy of all video sequences  $mSA$  is the final evaluation result.

Based on Center Location Error (CLE) and Overlap Ratio (OR), precision and success are introduced to measure the performance of a tracker under One Pass Evaluation (OPE). Precision is the percentage of the successful frame whose output location is within a given threshold (*e.g.*, 20 pixels). Success denotes the ratio of the successful frame whose overlap is larger than a given threshold.

**Protocol I.** Visible light or infrared video sequences are used to evaluate UAV trackers’ performance, respectively. Researchers can choose to use any training set except for those with UAV objects to boost trackers’ performance. It aims to verify the trackers’ performance for UAV tracking without the training of the UAV dataset. Moreover, it can demonstrate the generalization performance of trackers in Protocol I. Finally, the tracker is evaluated by the performance of visible light and infrared sequences, respectively. It is worth mentioning that attribute annotation is only for infrared video sequences.

**Protocol II.** Anti-UAV consists of visible light and infrared training set. Researchers can use visible or infrared training video sequences of Anti-UAV to finetune their trackers or train them from scratch. Protocol II aims to provide a unique UAV tracking evaluation of trackers. Because there are several options for researchers to choose from, so it is essential to point out which performance comes from training data settings. Otherwise, it will bring an unfair performance comparison.

**Protocol III.** Since Anti-UAV contains multiple modal data, researchers are encouraged to explore how to make the most of multi-modal data. The final performance is evaluated on both annotations of visible and infrared video sequences. Unlike the standard multi-modal tracking datasets published, the multi-modal data of Anti-UAV are not aligned, which is a new direction to explore using multi-modal data without alignment to track UAVs in the future.

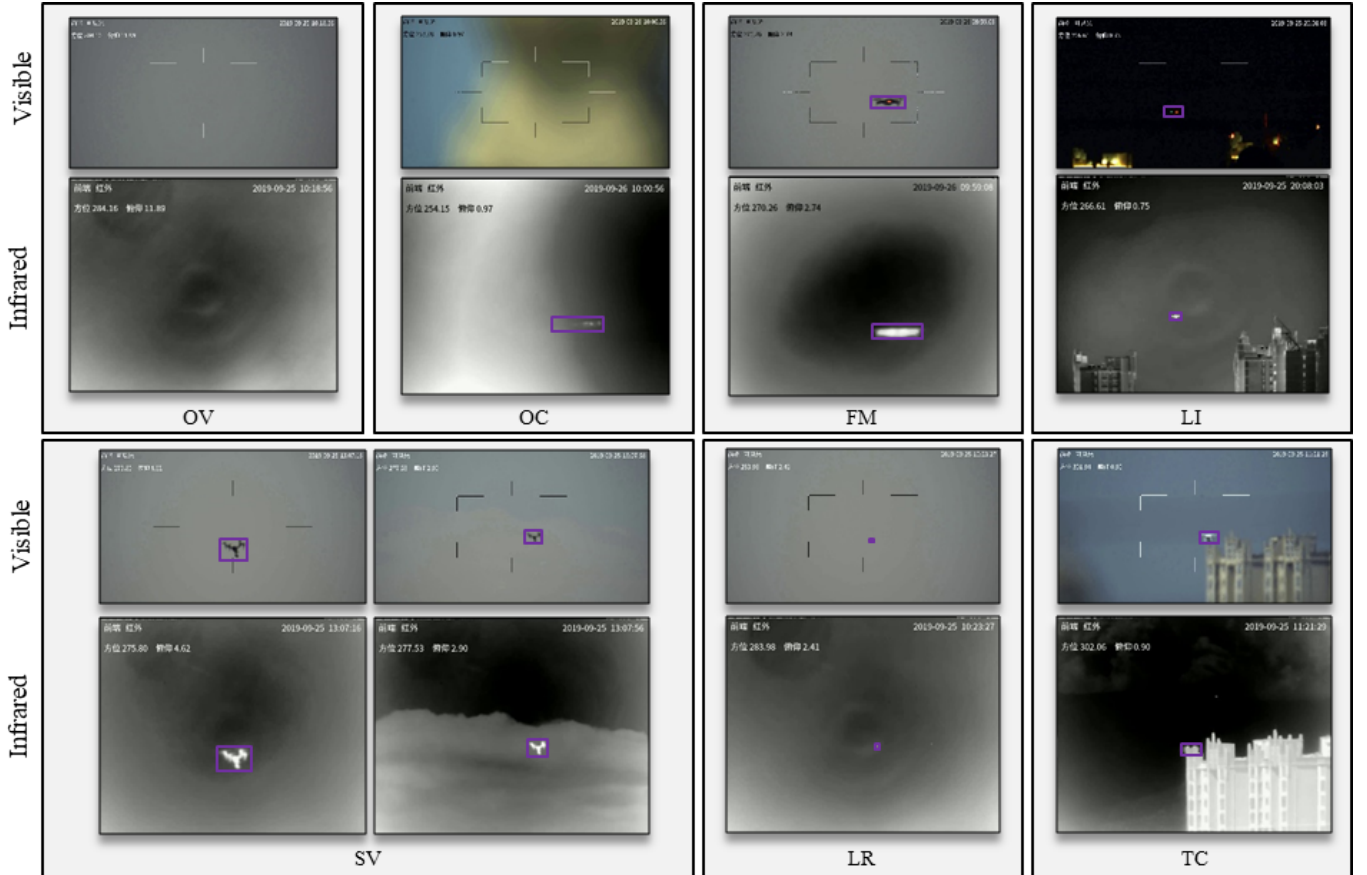


Fig. 5. Screenshots taken from Anti-UAV multi-modal dataset. The various attributes of the UAV dataset are illustrated in the figure, which are difficult problems in the tracking process. The various annotation attributes are more helpful for us to measure the current difficulties and challenges of UAV tracking, and also to analyze the shortcomings and advantages of the tracker from all aspects. It is worth mentioning that there is no alignment between multi-modal data, and the target location and size of the two may not be consistent.

#### IV. METHODOLOGY

**Motivation.** In this work, the proposed method is based on GlobalTrack [75], a baseline for long-term tracking. Although GlobalTrack is a simple yet effective tracker, further improvements can be made by taking accounts of the characteristics of Anti-UAV. There is only one class of objects in Anti-UAV dataset — UAVs. Therefore, even in different video sequences, the foreground information is related to each other. Inspired by this, training strategy can be enhanced. During training, the network can combine the features from different video sequences so that the obtained feature can be more robust. Based on this idea, dual-flow semantic consistency (DFSC) training strategy is proposed in this paper.

**Overview.** As shown in Fig. 8, dual-flow semantic consistency (DFSC) training strategy is composed of the following two modulation stages: class-level semantic modulation (CSM) stage and instance-level semantic modulation (ISM) stage. During the class-level semantic modulation stage, the feature map of search image is modulated by ROI features from different video sequences’ query images. In this case, the tracker will focus on not only the similar representation of UAV instance on current query image, but also potential representation of instances in entire UAV category. It is beneficial to increase the robustness of tracker since UAV on image may

experiences a considerable appearance change after several frames. After the CSM stage, the selected proposals will be used for the training of next stage — instance-level semantic modulation (ISM) stage. In this stage, these proposals will be only modulated by the ROI feature of the current video sequence’s query image. In the following, the DFSC training strategy is given in detail.

##### A. Class-level Semantic Modulation

The class-level semantic modulation stage is to find candidate boxes containing UAV category objects, which can be regarded as a UAV detection problem. The training strategy of the query guided region proposal network (query-guided RPN) as introduced in GlobalTrack is modified. The specific training strategy modulates the search area by using cross-sequence query. The general UAV modulation feature obtained in the CSM stage can be defined as  $\hat{t}$ . Specifically, the cross-sequence query modulation is defined as follows,

$$\hat{t}_{ij} = f_{CSM}(z_i, x_j) = f_{out}((f_z(z_i) \otimes f_x(x_j))), \quad (2)$$

where  $z_i$  denotes the ROI features of the query in  $i$ -th sequence,  $x_j$  denotes the feature of the search image of  $j$ -th sequence extracted from backbone. Specially,  $f_{CSM}$  is the modulator to modulate the intra-sequence and cross-sequence using different combinations of  $z_i$  and  $x_j$ .  $\hat{t}_{ij}$  retains the size

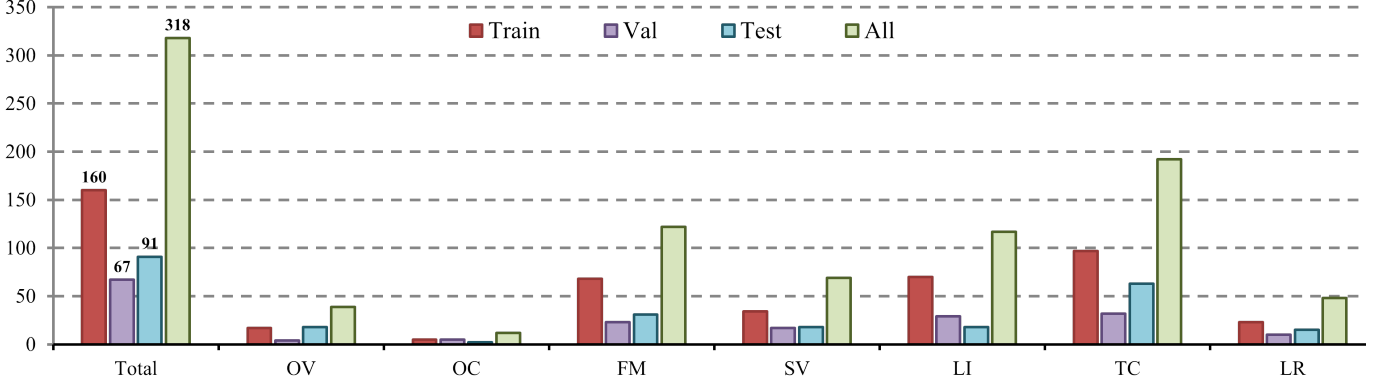


Fig. 6. The quantity of sequences with different attribute in Anti-UAV multi-modal dataset. Overall, the distributions of attributes in train, validation and test set are about the same. The attribute with most sequences is TC and the attribute with minimum sequences is OC.

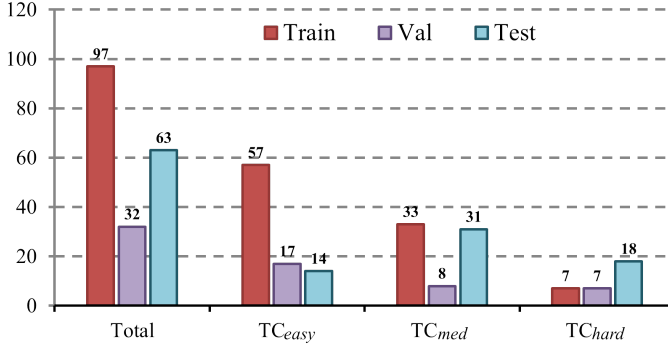


Fig. 7. Further division of attribute TC according to the complexity of tracking sequences. According to the performance of SiamRPN++ on the TC part, the complexity levels are divided into easy, med and hard.

of  $x_j$ , and it denotes the modulated feature which will be utilized to generate the proposals.  $f_{out}$  is utilized to align the feature channel number of  $\hat{t}_{ij}$  and  $x_j$ ,  $f_z$  and  $f_x$  respectively act on  $z_i$  and  $x_j$  to obtain the projected feature.  $\otimes$  represents convolution operator.

It is worth mentioning that the value range of  $i$  and  $j$  is between 0 and the current batch size  $n$ . When  $i$  and  $j$  are not equal, the cross sequence’s image modulation method will be adopted. When  $i$  and  $j$  are equal, the image modulation method is degenerated to the intra-sequence.

According to the above definition, the classification and regression part of the tracker are trained in the CSM stage. In the training, the loss function is defined as follows,

$$\begin{aligned}
 L_{CSM}(z_i, x_i, z_j, x_j) &= L_{same} + \alpha L_{cross} \\
 &= \sum_{i,j \in n, i=j} L_{rpn}(\hat{t}_{ij}) + \alpha \sum_{i,j \in n, i \neq j} L_{rpn}(\hat{t}_{ij}).
 \end{aligned} \quad (3)$$

Here  $\alpha$  is a weight coefficient for adjusting the ratio between  $L_{cross}$  and  $L_{same}$ . Both  $L_{cross}$  and  $L_{same}$  are loss functions of RPN. Here “cross” denotes RPN prediction after cross-sequence modulation while “same” denotes PRN prediction after intra-sequence modulation. Specifically, the training loss

function of RPN can be expressed as follows

$$L_{rpn}(\hat{t}_{ij}) = \frac{1}{N_{cls}} \sum_n L_{cls}(s_n, s_n^*) + \beta \frac{1}{N_{reg}} \sum_n L_{reg}(p_n, p_n^*). \quad (4)$$

Here  $\beta$  is a weight utilized to balance the classification and regression losses,  $s_n$  and  $s_n^*$  respectively represent the estimated classification score and corresponding groundtruth, while  $p_n$  and  $p_n^*$  are the location of the  $n$ -th proposal and the corresponding groundtruth.

### B. Instance-level Semantic Modulation

In the previous stage, proposals similar to UAV class are chosen. While in ISM stage, the emphasis is on instance-related information. At this point, the tracker aims to distinguish instance from those with similar appearance information or from complex background.

Given the query of the sequence to which the current feature belongs, proposals will be utilized for classification and bounding box refinement. The instance-level semantic modulation between  $z$  and  $x_k$  is performed as:

$$\hat{t}_k = f_{ISM}(z, x_k) = f'_{out}((f'_z(z) \odot f'_x(x_k))), \quad (5)$$

where  $x_k$  represents the selected  $k$ -th proposals and  $z$  represents the ROI feature of the query image that in the same sequence which the current feature  $x_k$  comes from.  $f_{ISM}$  is the modulator to modulate instance-special information into selected proposals.  $f'_{out}$  keeps  $\hat{t}_k$  and  $x_k$  the same size.  $f'_z$  and  $f'_x$  represent the feature projection modules for  $z$  and  $x_k$ , respectively.  $\odot$  denotes the Hadamard production.

Then, the traditional GlobalTrack QG-RCNN training processing is proceeded. The modulated ROI feature  $\hat{t}_k$  will be performed classification and regression to get the results of the tracker as follows,

$$L_{ISM}(z, x) = \frac{1}{N_{pnum}} \sum_k L_{rcnn}(\hat{t}_k). \quad (6)$$

Here  $N_{pnum}$  denotes the number of the selected proposals from the CSM stage. For every modulated ROI feature  $\hat{t}_k$ , the loss function can be formulated as

$$L_{rcnn}(\hat{t}_k) = L'_{cls}(s'_n, s'^*_n) + \beta L'_{reg}(p'_n, p'^*_n), \quad (7)$$



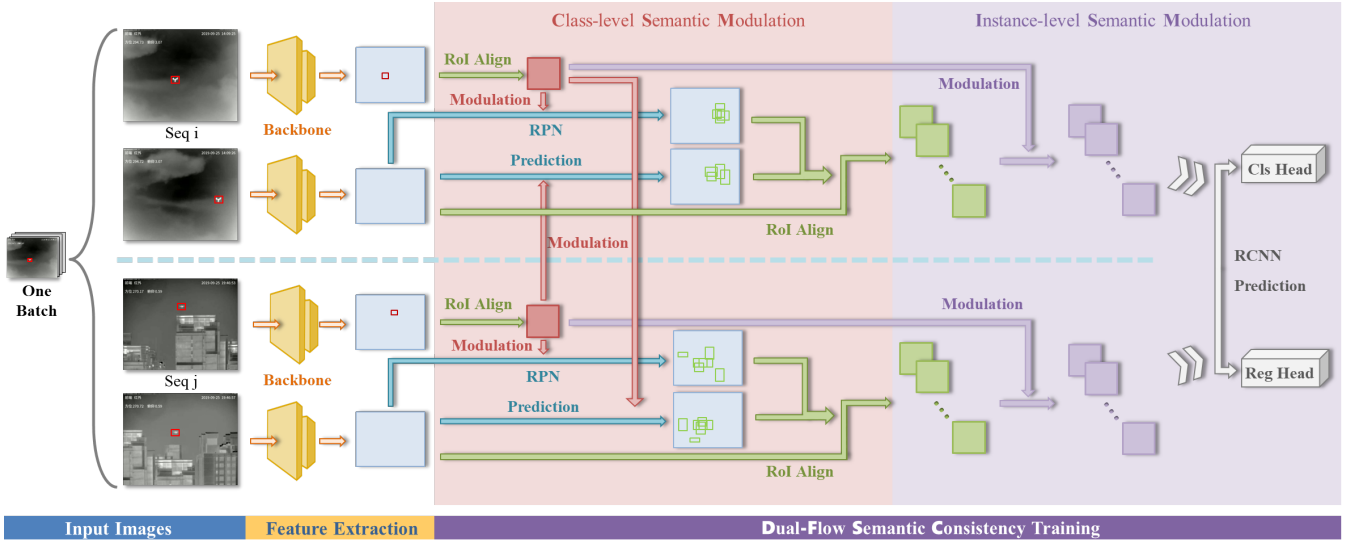


Fig. 8. The pipeline of proposed dual-flow semantic consistency training strategy (DFSC). This figure shows the case when two video sequences (denoted as Seq i and Seq j) in a batch. During the training process, each training sample has a UAV on it. Given the sequence pairs, the tracker is enabled to enhance specific capabilities at different stages. There are two semantic information modulation branches in the whole DFSC training process, including class-level semantic modulation (CSM) and instance-level semantic modulation (ISM). To reduce the intraclass differences, cross sequence UAV features are used as modulation factors to maintain class-level semantic information consistency in the CSM stage. During the ISM stage, the modulation of the query feature of the same sequence further boosts the tracker’s discrimination power by reinforcing instance-level semantic consistency. It is worth mentioning that the cross-modulation used in the whole strategy share most computation. Only the training process is adopted by the DFSC method, which makes no burden on inference time. Best viewed in color.

where  $s'_n$  and  $s_n^*$  represent the predicted confidence score and corresponding groundtruth, respectively.  $p'_n$  and  $p_n^*$  are the location of the  $n$ -th proposal and the corresponding groundtruth.

## V. EXPERIMENTS

Extensive experiments are conducted on the Anti-UAV for performance analysis in this section.

### A. Trackers

Deep learning based trackers [12–16, 25, 62, 63, 74, 75, 88, 90–98] and correlation filters based trackers [19, 49–51, 53, 55, 60, 81–87, 89] are used for comparison in this paper. The baseline tracker evaluated in the benchmark is briefly described below. The performance of the following trackers has not been fine-tuned on the Anti-UAV training set.

Deep learning based trackers need to train on large-scale datasets. In recent years, due to the rapid development of deep learning and hardware, object tracking based on deep learning has made great progress. In this section, different kinds of trackers are introduced. Siamese network family occupies a very important position in the field of single object tracking.

### B. Implementation Details

**Hyper-parameters.** For protocol II, GlobalTrack is utilized as the baseline for demonstrating the effectiveness of the DFSC algorithm. There are two settings of hyper-parameters for visible and infrared dataset, respectively.

For Anti-UAV visible dataset, the pre-trained model provided by GlobalTrack is utilized as the initial model. There are 12 epochs in total, and the initial learning rate is set to 0.02,

which is then set to 0.002 and 0.0002 at the 8th epoch and the 11th epoch, respectively. Concerning Anti-UAV infrared dataset, the initial weights transferred from Faster RCNN are adopted and then trained with 18 epochs. The learning rate is also set to 0.02, and we decay it to 0.002 and 0.0002 at the 12th, 15th epoch, respectively.

In the training phase of CSM and ISM, the classification and regression losses are respectively cross-entropy and smooth L1, while the batch size is set to 2 per GPU.

**Training Set.** Only the Anti-UAV infrared dataset is used in the training of infrared UAV tracker. However, in the visible UAV tracker training, the pre-trained GlobalTrack model utilizes a combination of MS COCO [99], LaSOT and GOT-10k. During the finetune stage, only the Anti-UAV visible dataset is adopted for training.

MS COCO is an object detection dataset containing over 118 thousand images and 80 object classes. The details of LaSOT and GOT-10k can be found in Section II-A.

### C. Evaluations under Protocol I

**Overall Performance.** Fig. 9 shows the success plot and the precision plot of one pass evaluation (OPE) on Anti-UAV. SiamRCNN achieves the best precision score of 95.70% and a success score of 71.52% on the infrared validation set. Furthermore, SiamRCNN also obtains state-of-the-art results with a 63.60% success score on the infrared test set. GlobalTrack shows top performance with precision score of 87.13% on the infrared test set. Moreover, SiamRCNN achieves more remarkable performance improvement than the infrared tracking sequence on the visible tracking sequence. For instance, SiamRCNN outperforms 4.68 points in success score and 3.06

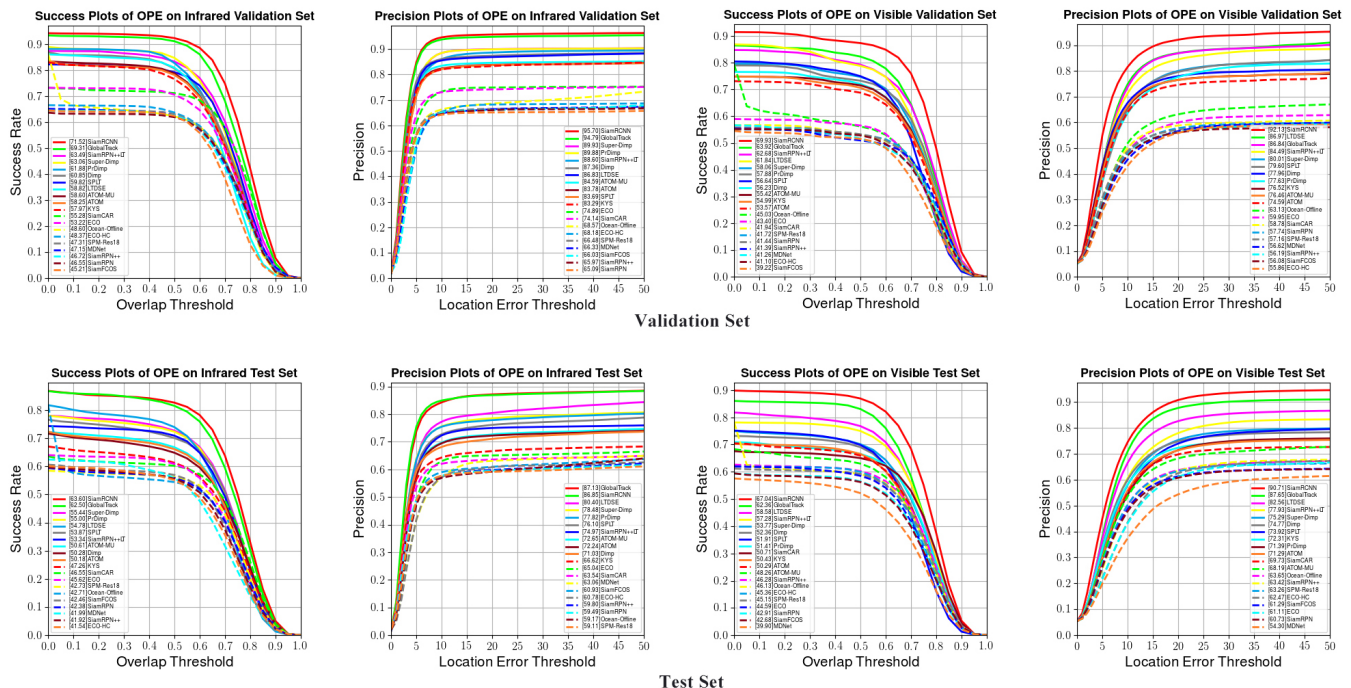


Fig. 9. The success plot and precision plot on Anti-UAV under protocol I. In both cases, the evaluation performances of SiamRCNN and GlobalTrack are more than any other tracker by a large margin. For clarity, only the top 20 trackers are shown. Best viewed in color.

points in precision score over the second tracker GlobalTrack on the visible test set. However, it is worth mentioning that the inference speed of SiamRCNN is far slower than other trackers. Taking the infrared test set as an example, ECO-HC is the best correlation filter tracker with a 60.78% precision score and a 41.54% success score. The best deep tracker with online learning is Super-Dimp with 78.48% precision score and 55.44% success score.

In Tab. III and Tab. IV, each tracker is used without any modification. The evaluation results in  $mSA$  (%) is given. For infrared sequence, SiamRCNN achieves the best state accuracy score of 74.33% on the validation set and 65.41% on the test set. According to the experimental results, the tracker based on long-term tracking is more likely to achieve higher performances. The long-term tracker’s underlying assumption is that tracking the target out of view is possible. In this setting, long-term tracking will generally have a larger search area or search in the whole image to enable the tracker to obtain the vanishing target reappearing position.

Nevertheless, the above mentioned long-term tracker is challenging to achieve a real-time requirement. The order of the tracker is from low to high according to the performance on the test set. Trackers based on deep learning generally have a higher performance. In most cases, UAV tracking under visible light video sequence has a better solution.

**Attribute-based Performance.** To analyze different challenges faced by existing trackers, all trackers are evaluated on seven attributes. The results of several challenging attributes are shown in Tab. III and Tab. IV.

For instance,  $OV$  generally does not appear in the short-term tracker setting. The short-term tracking sequence is

usually not as long as the sequence in the Anti-UAV dataset. Meanwhile, because the UAV is generally far away from the camera, it is also challenging to track such a small target. Therefore, many trackers do not perform well on video sequences with  $LR$  attribute, especially correlation filter tracker, due to the trackers’ anchor setting; after all, UAVs’ size in Anti-UAV is usually too small. Tracking sequences with  $TC$  attribute make up a large part of Anti-UAV.  $TC_{easy}$ ,  $TC_{med}$  and  $TC_{hard}$  is generated by the tracking difficulty of the corresponding infrared sequence. Without color and texture information, UAVs are easily confused with complex backgrounds and distractors in similar temperature scenes. So another challenge is to determine the location of the UAV in this complex scene. It is shown that  $TC_{hard}$  is the most challenging attribute. When tracking UAVs in the video sequences with  $TC_{hard}$  attribute, it is not easy to distinguish the UAV from the buildings without fine-tuning using the Anti-UAV training set.

On most attributes, SiamRCNN and GlobalTrack perform much better than other trackers for their more sophisticated processing designs on every frame. On the test set, these two trackers achieve comparable performance except for  $FM$ ,  $LR$  and  $LI$ . The superiority that over 4.00%  $mSA$  of the above three attributes makes SiamRCNN a lead. And on  $OV$  and  $SV$ , GlobalTrack is slightly ahead while it is reverse on  $TC$ . As for the validation set, GlobalTrack has a slight lead over the second tracker on  $OC$  and  $LI$ . While the performances of SiamRCNN on other attributes are all the best. Especially on  $OV$ ,  $TC$  and  $LR$ , SiamRCNN performs far better than that of other trackers. Thus it can be seen that SiamRCNN performs well on each of the seven attributes.

TABLE III

THE WHOLE ATTRIBUTE-BASED PERFORMANCES  $mSA$  (%) OF BASELINE TRACKERS ON ANTI-UAV VALIDATION SET USING THE EVALUATION PROTOCOL I. THE TRACKERS ARE RANKED IN THE SAME WAY AS IN TAB. VI. LARGER NUMBER MEANS BETTER PERFORMANCE. THE **FIRST**-, **SECOND**- AND **THIRD**-PLACE TRACKERS ARE LABELED WITH RED, BLUE AND GREEN COLORS RESPECTIVELY. BEST VIEWED IN COLOR.

Tracker	Infrared										Visible	
	OV	OC	FM	SV	LI	TC				LR	All	All
						$TC_{easy}$	$TC_{med}$	$TC_{hard}$	$TC_{all}$			
MOSSE [49]	23.29	4.63	5.26	8.08	28.64	48.70	27.19	8.17	34.45	6.20	29.40	21.06
DAT [81]	15.98	6.77	8.30	9.63	30.76	36.06	20.62	1.49	24.64	3.00	29.43	38.27
CSK [50]	21.33	8.90	6.02	8.06	40.32	53.32	44.70	7.51	41.14	1.96	37.67	35.89
Staple-CA [82]	21.33	10.65	7.09	14.09	36.96	55.63	46.81	14.54	44.43	10.48	37.51	37.23
MCCTH [19]	26.51	20.61	8.65	17.80	39.75	54.28	42.12	8.81	41.29	10.29	38.10	39.49
Staple [51]	33.92	13.82	7.54	17.64	36.20	54.80	40.54	13.01	42.09	9.81	37.62	38.15
DCF-GRAY [55]	34.84	10.86	13.66	20.33	39.90	49.84	36.25	7.31	37.14	14.36	38.77	31.26
CN [53]	24.74	10.12	6.93	14.74	40.78	58.34	46.32	11.22	45.03	10.25	39.82	36.04
KCF-GRAY [55]	44.49	13.17	14.69	26.08	46.02	58.47	43.98	12.48	44.79	16.66	44.37	31.80
DCF [55]	21.15	6.93	6.95	13.32	37.57	53.64	42.68	9.02	41.14	11.44	36.65	36.48
KCF [55]	22.04	8.85	7.50	14.21	37.91	53.41	42.94	9.67	41.23	11.92	36.82	38.11
STRCF [83]	39.25	25.34	21.56	27.04	48.48	47.92	41.02	4.47	36.69	18.34	41.65	44.92
LDES [84]	21.76	8.91	19.78	13.55	46.63	54.01	42.90	5.05	40.52	8.92	41.41	48.98
DSST [85]	23.66	10.46	7.05	14.03	43.25	55.31	45.76	13.55	43.79	9.29	40.54	37.48
CSRDCF [86]	40.46	21.13	25.45	27.84	50.87	58.66	52.17	14.53	47.39	24.77	47.73	41.54
DSST-LP <sup>1</sup>	22.31	11.30	8.27	15.25	44.03	54.50	48.61	14.14	44.20	9.71	41.03	36.86
BACF [87]	19.51	9.00	18.21	20.53	44.72	56.47	44.43	7.06	42.65	21.99	43.16	43.87
SiamFC [12]	42.10	27.99	30.28	22.83	53.41	66.36	45.80	10.45	48.99	16.59	49.34	44.08
Ocean-Online [88]	16.21	21.02	19.65	24.11	45.77	52.66	39.21	6.09	39.11	20.33	41.56	46.45
MKCFup [89]	44.60	20.13	8.64	22.57	40.81	56.95	43.91	13.77	44.24	10.25	41.31	40.21
SiamMask [15]	40.77	27.28	24.22	24.16	47.10	54.82	38.76	12.50	41.54	14.62	44.34	44.26
SiamDW [90]	43.93	39.66	29.40	35.14	56.84	59.89	42.31	8.29	44.21	27.87	49.46	44.90
MKCFup-LP <sup>1</sup>	43.74	11.39	6.48	19.28	41.94	57.22	46.76	14.30	45.21	9.66	42.28	40.19
SiamBAN [91]	20.02	31.73	19.03	24.84	48.75	57.63	49.44	6.44	44.39	13.38	43.60	39.90
RT-MDNet [62]	43.88	20.82	18.60	27.35	46.97	64.97	44.42	13.15	48.50	13.52	45.99	44.93
SPM-AlexNet [74]	39.84	24.75	30.35	27.70	51.15	56.73	34.98	8.20	40.68	14.41	46.71	46.51
ECO-HC [60]	23.16	14.96	25.38	28.66	52.66	60.61	48.51	16.63	47.96	30.29	49.26	43.67
Ocean-Offline [88]	26.63	42.86	32.09	24.75	55.05	59.61	41.66	20.76	46.62	18.60	48.74	45.74
MDNet [63]	45.88	24.16	23.47	31.13	50.42	65.96	48.59	14.84	50.43	24.85	49.49	45.17
SiamRPN++ [14]	35.32	41.11	28.17	28.39	55.85	57.95	44.55	6.94	43.44	19.71	48.60	46.12
SiamRPN [13]	32.07	31.37	25.73	30.56	52.57	65.60	45.24	10.83	48.53	21.97	48.16	46.63
SPM-Res18 [74]	39.75	30.78	32.25	29.56	54.90	59.16	42.55	12.45	44.79	17.95	49.56	46.09
SiamFCOS [25]	41.97	42.43	29.01	34.66	53.09	58.24	37.02	10.07	42.40	21.94	47.71	44.28
ECO [60]	31.87	32.03	38.43	38.47	55.77	69.24	45.90	21.67	53.00	34.25	54.44	46.31
SiamCAR [92]	25.05	46.12	40.84	29.96	63.19	68.27	55.99	17.55	54.11	21.67	56.70	46.52
KYS [93]	36.07	55.52	57.64	52.68	64.70	66.30	35.35	32.05	51.07	48.00	60.50	59.79
ATOM [16]	63.01	55.82	56.04	46.91	65.05	65.36	50.03	25.73	52.86	38.53	60.87	58.79
Dimp [94]	41.96	59.85	59.95	55.78	66.33	70.19	51.62	30.16	56.79	47.52	63.51	61.54
ATOM-MU [95]	42.73	55.51	58.74	47.16	64.83	68.58	46.61	26.26	53.83	39.18	61.27	60.45
SiamRPN++LT [14]	50.02	<b>68.16</b>	63.39	54.06	<b>70.25</b>	<b>76.71</b>	<b>61.76</b>	19.25	<b>60.40</b>	42.66	<b>65.84</b>	<b>67.15</b>
SPLT [96]	33.39	58.42	55.22	42.49	63.18	73.09	58.73	19.30	57.73	45.46	60.73	57.32
PrDimp [97]	<b>65.22</b>	63.89	62.85	55.59	66.95	69.47	55.79	29.04	57.21	51.12	64.54	62.95
LTDSE [25]	64.39	50.17	59.04	48.67	62.69	67.18	55.89	27.43	55.66	42.54	61.27	66.64
Super-Dimp <sup>2</sup>	52.35	68.07	<b>65.30</b>	<b>64.80</b>	67.93	68.87	59.85	<b>34.22</b>	59.03	<b>61.45</b>	65.76	63.05
GlobalTrack [75]	<b>69.21</b>	<b>78.62</b>	<b>73.35</b>	<b>66.11</b>	<b>76.33</b>	<b>76.47</b>	<b>63.08</b>	<b>43.45</b>	<b>65.90</b>	<b>60.26</b>	<b>72.00</b>	<b>67.28</b>
SiamRCNN [98]	<b>73.46</b>	<b>78.24</b>	<b>73.98</b>	<b>67.97</b>	<b>76.19</b>	<b>78.21</b>	<b>69.55</b>	<b>55.48</b>	<b>71.07</b>	<b>67.93</b>	<b>74.33</b>	<b>74.32</b>

#### D. Evaluation under Protocol II

Here, the finetuning of the GlobalTrack model only with Anti-UAV directly is defined as the normal training strategy. Otherwise, finetuning the GlobalTrack model using the DFSC method only with Anti-UAV is called the DFSC training strategy. The model provided on GitHub is called the large-scale training strategy, which utilizes MS COCO, LaSOT, and GOT-10k as the training set.

**Overall Performance.** As shown in Tab. V, DFSC obtains the best performance on both infrared and visible sequences. Compared with the normal training strategy, DFSC gains a 0.49  $mSA$  gain on the validation set and 0.68  $mSA$  gain

on the test set for the infrared dataset. For visible tracking sequence, DFSC improves  $mSA$  by 0.48 on the validation set and 0.57 on the test set, respectively. And compared with large-scale training strategy, the normal and DFSC methods gain obviously on validation set. This is because in Anti-UAV, the sequences in training set and validation set may come from the same video. Through the learning of similar data, the tracker can make a more accurate judgment. However, since test set is independent of the other two sets, the performance gains of normal and DFSC method decrease on test set, showing that the tracker is overfitting in the training set to some extent.

Similar observations can be obtained in the metric comparison among different methods on precision and success. Tab. VII shows the results, which demonstrates that the proposed

<sup>1</sup><https://github.com/fengyang95/pyCFTrackers>

<sup>2</sup><https://github.com/visionml/pytracking>

TABLE IV

THE WHOLE ATTRIBUTE-BASED PERFORMANCES  $mSA$  (%) OF BASELINE TRACKERS ON THE ANTI-UAV TEST SET USING THE EVALUATION PROTOCOL I. THE TRACKERS ARE RANKED BY THEIR STATE ACCURACY SCORES OF INFRARED VIDEO ON TEST SET. LARGER NUMBER MEANS BETTER PERFORMANCE. THE **FIRST**-, **SECOND**- AND **THIRD**-PLACE TRACKERS ARE LABELED WITH RED, BLUE AND GREEN COLORS RESPECTIVELY. BEST VIEWED IN COLOR.

Tracker	Infrared										Visible	
	OV	OC	FM	SV	LI	TC				LR	All	All
						$TC_{easy}$	$TC_{med}$	$TC_{hard}$	$TC_{all}$			
MOSSE [49]	8.89	24.16	6.02	4.06	3.56	15.23	10.34	5.80	10.13	3.80	13.47	15.23
DAT [81]	8.01	21.94	5.33	13.53	3.11	40.57	13.28	6.50	17.41	3.76	22.68	27.19
CSK [50]	11.51	26.97	9.56	12.35	2.71	46.51	15.63	5.30	19.54	3.29	24.26	28.38
Staple-CA [82]	15.60	41.11	13.29	9.03	3.64	46.25	18.27	7.38	21.37	5.53	25.44	31.40
MCCTH [19]	11.58	33.21	9.84	9.08	4.95	41.09	20.33	6.61	21.02	5.13	25.85	29.96
Staple [51]	14.74	44.09	11.56	11.67	3.70	44.56	21.51	6.82	22.44	5.26	26.50	29.71
DCF-GRAY [55]	14.59	36.84	13.36	15.66	3.55	64.22	22.08	7.66	27.33	4.12	30.81	31.67
CN [53]	14.41	39.75	10.66	15.18	3.54	59.75	28.02	7.93	29.33	4.81	31.72	28.65
KCF-GRAY [55]	10.16	34.96	12.18	16.04	3.98	59.20	24.29	9.75	27.89	4.68	31.86	30.83
DCF [55]	14.85	36.89	12.28	11.55	3.18	60.32	30.26	8.80	30.80	4.25	32.55	38.39
KCF [55]	16.14	37.56	12.60	11.66	3.55	60.23	30.80	9.17	31.16	4.36	32.88	39.40
STRCF [83]	15.72	44.39	14.69	20.18	7.31	59.49	28.26	10.89	30.23	7.84	33.77	45.19
LDES [84]	16.83	40.97	17.86	16.33	8.40	60.88	28.07	10.46	30.33	7.54	34.46	49.13
DSST [85]	14.45	41.19	12.59	15.88	3.57	69.31	30.86	9.37	33.27	4.85	35.18	35.67
CSRDCF [86]	13.70	46.26	12.96	19.14	4.97	61.55	32.05	10.22	32.37	7.26	35.29	47.10
DSST-LP <sup>1</sup>	17.23	40.86	12.79	17.58	3.99	70.59	31.84	8.85	33.88	5.31	35.70	35.88
BACF [87]	16.17	41.91	15.66	16.70	4.13	70.16	33.02	8.53	34.28	4.91	36.78	47.52
SiamFC [12]	18.59	60.83	21.46	23.58	13.55	63.82	29.00	11.02	31.60	10.36	36.97	45.69
Ocean-Online [88]	17.98	41.56	14.72	17.35	3.73	68.51	32.02	9.27	33.63	4.45	37.22	48.11
MKCFup [89]	16.44	43.35	15.60	14.15	3.48	70.74	35.55	8.92	35.76	4.88	37.41	39.52
SiamMask [15]	29.09	53.55	18.73	22.03	8.14	59.32	30.42	17.91	33.27	10.08	37.44	45.92
SiamDW [90]	19.36	38.14	17.65	22.18	8.52	57.68	36.28	13.73	34.60	9.44	38.01	49.86
MKCFup-LP <sup>1</sup>	17.34	45.04	15.12	15.26	3.51	71.56	38.10	8.15	36.98	4.99	38.58	39.90
SiamBAN [91]	14.92	33.72	16.42	18.84	4.78	72.67	39.33	16.90	40.33	6.15	40.86	44.71
RT-MDNet [62]	19.66	50.00	20.88	21.38	12.42	65.38	37.37	16.21	37.55	7.98	41.05	42.59
SPM-AlexNet [74]	28.82	54.65	22.99	21.89	10.96	72.10	35.75	16.00	38.19	10.86	41.33	54.09
ECO-HC [60]	20.48	50.46	20.72	24.69	6.74	77.18	41.74	14.76	41.91	10.21	42.39	48.91
Ocean-Offline [88]	25.11	53.63	23.74	21.07	12.22	71.65	40.67	9.26	38.58	10.74	42.51	47.45
MDNet [63]	28.90	73.29	24.19	20.60	12.95	65.92	42.13	15.44	39.79	12.14	42.95	43.94
SiamRPN++ [14]	22.96	48.88	20.44	21.27	9.63	75.16	40.24	16.46	41.21	10.76	43.01	51.69
SiamRPN [13]	25.35	46.57	24.50	21.90	14.92	74.95	39.37	11.54	39.32	11.18	43.39	47.96
SPM-Res18 [74]	27.02	55.47	23.73	26.13	10.85	76.39	40.14	14.16	40.77	12.92	44.06	50.42
SiamFCOS [25]	28.74	53.54	23.39	26.24	10.81	73.10	42.28	17.89	42.16	12.40	44.37	48.54
ECO [60]	24.38	45.92	23.90	23.36	11.38	75.76	48.21	14.72	44.76	7.97	46.51	47.31
SiamCAR [92]	28.90	48.06	29.03	27.63	17.82	78.88	45.27	13.01	43.52	12.52	47.82	54.79
KYS [93]	40.80	55.25	35.23	35.70	33.30	73.71	46.77	17.58	44.42	24.61	49.32	55.85
ATOM [16]	40.17	53.91	36.45	34.39	36.70	73.24	54.37	23.58	49.77	25.84	52.19	55.68
Dimp [94]	40.87	55.29	36.57	40.03	32.42	73.53	48.82	29.93	48.91	25.57	52.47	58.25
ATOM-MU [95]	38.67	53.84	35.37	35.73	35.44	74.30	52.16	26.81	49.84	24.85	52.61	54.02
SiamRPN++LT [14]	45.50	71.71	47.09	43.61	44.70	75.88	52.75	18.66	48.15	32.35	54.34	61.17
SPLT [96]	49.92	51.73	51.75	41.69	54.76	72.46	50.82	26.39	48.65	37.89	54.63	53.10
PrDimp [97]	57.43	79.52	49.40	50.05	49.09	74.29	53.68	31.43	51.90	37.42	56.50	57.02
LTDSE [25]	56.25	75.55	53.65	49.89	56.72	71.19	52.04	37.79	52.22	48.70	56.51	64.29
Super-Dimp <sup>2</sup>	53.37	78.79	46.59	47.45	46.77	75.39	56.50	31.99	53.69	35.58	57.72	59.49
GlobalTrack [75]	68.98	79.47	63.42	57.34	67.78	74.38	60.24	43.02	58.46	58.48	63.86	66.24
SiamRCNN [98]	68.17	78.49	67.66	57.23	73.92	78.78	61.89	42.48	60.10	64.04	65.41	70.83

TABLE V

COMPARISONS IN TERMS OF  $mSA$  (%) WITH THE BASELINE TRACKER GLOBALTRACK. THE LARGE-SCALE TRAINING STRATEGY UTILIZES MS COCO, LASOT, AND GOT-10K AS THE TRAINING SET. THE NORMAL TRAINING STRATEGY IS DEFINED AS DIRECTLY FINETUNING THE GLOBALTRACK MODEL ONLY WITH ANTI-UAV. THE **BOLD** INDICATES THE BEST PERFORMANCE ON CORRESPONDING DATASET.

Method	Type	Infrared										Visible	
		OV	OC	FM	SV	LI	TC				LR	All	All
							$TC_{easy}$	$TC_{med}$	$TC_{hard}$	$TC_{all}$			
large-scale	val	69.21	78.62	73.35	66.11	76.33	76.47	63.08	43.45	65.90	60.26	72.00	67.28
normal		<b>78.09</b>	81.42	78.66	76.61	79.95	81.23	76.56	74.04	78.49	73.55	79.60	73.25
DFSC (Ours)		77.72	<b>82.70</b>	<b>79.34</b>	<b>77.58</b>	<b>80.31</b>	<b>81.48</b>	<b>76.83</b>	<b>75.65</b>	<b>79.04</b>	<b>74.33</b>	<b>80.09</b>	<b>73.73</b>
large-scale	test	68.98	<b>79.47</b>	<b>63.42</b>	<b>57.34</b>	<b>67.78</b>	74.38	60.24	43.02	58.46	<b>58.48</b>	63.86	66.24
normal		<b>70.44</b>	68.94	60.66	55.48	59.78	77.07	64.64	44.61	61.68	52.94	65.36	69.27
DFSC (Ours)		70.16	68.07	60.95	55.55	60.13	<b>77.96</b>	<b>65.85</b>	<b>45.59</b>	<b>62.75</b>	53.10	<b>66.04</b>	<b>69.84</b>

TABLE VI

ABLATION STUDY IN TERMS OF  $mSA$  (%) ON THE TEST SET WITH THE BASELINE TRACKER GLOBALTRACK. DFSC-ALL REPRESENTS THAT ISM STAGE USES THE SAME CLASS-LEVEL MODULATION AS CSM. DFSC MEANS THAT BOTH CLASSIFICATION AND REGRESSION TASKS ARE USED IN THE CSM PERIOD. DFSC-CLS AND DFSC-REG DENOTE ONLY CORRESPONDING TASK IS INTRODUCED UNDER THE SAME CONDITIONS. THE RATIO  $\alpha$  IS A WEIGHT TO BALANCE  $L_{cross}$  AND  $L_{same}$  AS SHOWN IN EQ. 3. THE **BOLD** INDICATES THE BEST PERFORMANCE.

Method	Infrared										Visible	
	OV	OC	FM	SV	LI	TC				LR	All	All
						$TC_{easy}$	$TC_{med}$	$TC_{hard}$	$TC_{all}$			
DFSC-all	68.26	66.23	58.66	54.60	56.96	77.38	63.65	44.14	61.12	50.51	63.99	67.94
DFSC-cls	70.22	<b>68.47</b>	60.78	55.49	60.02	<b>78.17</b>	65.75	45.07	62.60	52.29	<b>66.12</b>	69.53
DFSC-reg	<b>70.31</b>	68.26	60.70	55.31	59.05	77.52	65.52	<b>46.74</b>	<b>62.82</b>	51.76	66.06	68.95
DFSC	70.16	68.07	<b>60.95</b>	<b>55.55</b>	<b>60.13</b>	77.96	<b>65.85</b>	45.59	62.75	<b>53.10</b>	66.04	<b>69.84</b>
DFSC- $\alpha$ 0 (normal)	70.44	68.94	60.66	55.48	59.78	77.07	64.64	44.61	61.68	52.94	65.36	69.27
DFSC- $\alpha$ 0.25	<b>70.63</b>	<b>69.18</b>	60.80	<b>55.74</b>	59.61	<b>78.56</b>	65.70	<b>46.26</b>	<b>63.00</b>	52.75	<b>66.33</b>	<b>70.31</b>
DFSC- $\alpha$ 0.5	70.37	68.32	60.20	55.01	58.86	77.17	64.49	45.28	61.82	51.52	65.25	69.55
DFSC- $\alpha$ 1	70.16	68.07	<b>60.95</b>	55.55	<b>60.13</b>	77.96	<b>65.85</b>	45.59	62.75	<b>53.10</b>	66.04	69.84
DFSC- $\alpha$ 2	69.76	68.19	60.46	55.20	59.53	77.57	65.43	45.42	62.41	52.85	65.61	69.98

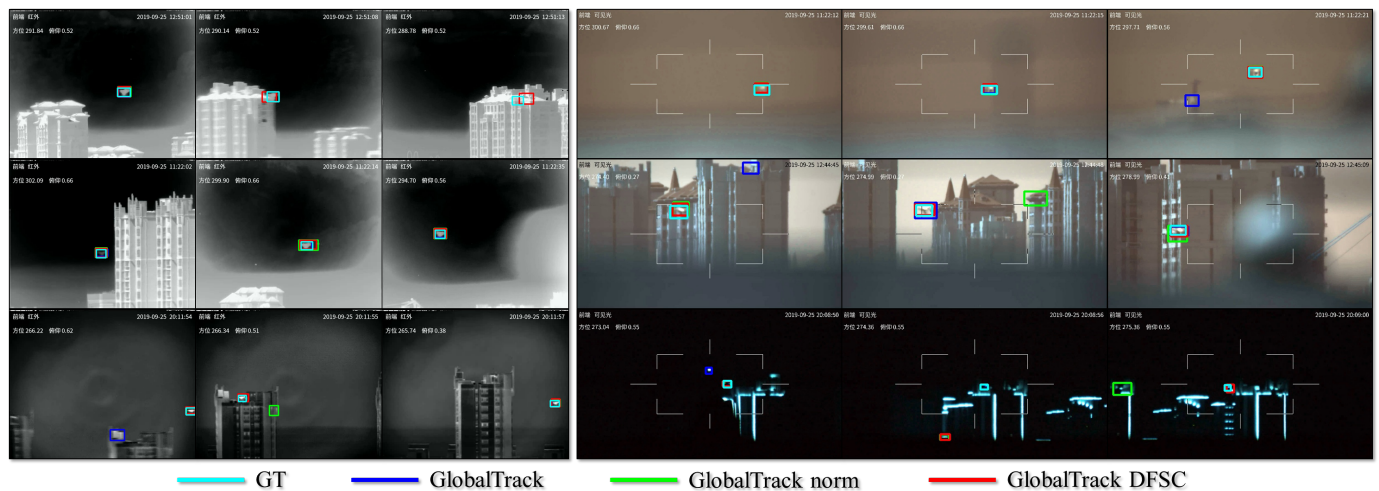


Fig. 10. A comparison of proposed DFSC with other method in protocol II. For example, on the left side of the second line, DFSC has a higher status accuracy rate in the face of complex background. On the contrary, finetune determines that there is no UAV in the scene at this time. Through the visualization of successful infrared and visible tracking sequences, respectively, it is shown that the proposed method successfully handles these challenges and provides accurate UAV state estimation. Best viewed in color.

TABLE VII

COMPARISON OF DIFFERENT TRAINING STRATEGY IN TERMS OF PRECISION (%) AND SUCCESS (%) ON INFRARED AND VISIBLE DATASET, RESPECTIVELY. THE **BOLD** INDICATES THE BEST PERFORMANCE ON CORRESPONDING DATASET.

Method	Infrared		Visible	
	Precision	Success	Precision	Success
large-scale	85.34	61.13	88.53	63.00
normal	87.61	62.88	93.30	65.22
DFSC	87.77	63.24	<b>93.87</b>	65.87
DFSC-all	86.97	61.59	91.87	64.20
DFSC-cls	87.47	63.14	93.72	65.56
DFSC-reg	<b>87.87</b>	63.35	93.26	65.24
DFSC- $\alpha$ 0.25	87.52	<b>63.40</b>	93.65	<b>66.24</b>
DFSC- $\alpha$ 0.5	87.08	62.53	93.84	65.66
DFSC- $\alpha$ 2	87.83	62.81	93.74	65.94

DFSC gets consistent performance improvement.

**Attribute-based Performance.** Different training strategies are evaluated on the defined attribute annotations to analyze the advantages and shortcomings of the proposed method on special attributes. Tab. V shows that the proposed method

improves the performance of most attributes on the validation set, especially  $OC$ . Compared with the normal training strategy, DFSC gains the  $mSA$  by 1.28%, 0.97% and 0.78% on  $OC$ ,  $SV$  and  $LR$ , respectively. In other attributes, performance improvement is limited.

Moreover, for the test set, DFSC gets the best  $mSA$  score (62.75%) on  $TC_{all}$ , which is higher than the normal training strategy by 1.07%. Compared with normal training strategy, DFSC gains the  $mSA$  by 0.89%, 1.21% and 0.98% and on  $TC_{easy}$ ,  $TC_{med}$  and  $TC_{hard}$ , respectively.

On the test set, the large-scale training strategy achieves the highest performance in most attributes except  $TC$  and  $OV$ . However, the whole performance is not as good as DFSC on  $mSA$ . On the one hand, the large-scale training strategy uses more data than the normal and DFSC method, which is conducive to learning more general features beneficial to tracking UAVs. Training on multiple large-scale datasets will improve the generalization ability of the tracker. On the other hand, after training on the Anti-UAV training set, the tracker has a more discrimination ability on  $TC$  scenarios and is more stable in common scenarios.

To validate the proposed DFSC method, the successful tracking sequences from test set are visualized, as shown in Fig. 10. As a consequence, a potential training strategy is demonstrated to handle such great challenges.

### E. Ablation Study

This subsection provides the analysis about the behaviors of the supervised task and  $\alpha$  in Eq. 3 for the dual-flow semantic modulation (DFSC) training strategy.

**Supervised Task.** As shown at the top half of Tab. VI, compared with other methods, DFSC-cls achieves the best performance on  $mSA$ , but has the lowest performance on success and precision on the infrared dataset. Nevertheless, DFSC-cls only gets a small margin over DFSC. Instead, DFSC-reg obtains a lower  $mSA$  but the highest precision and success scores. DFSC-cls makes the tracker own a more accurate UAV state discrimination ability, but its localization ability is not improved relatively. It validates the classification supervised task in the DFSC method to force the tracker to focus on the powerful capability of UAV perception. On the contrary, more attention to the regression task makes the tracker perform better on UAV localization.

Compared with the DFSC method, DFSC-all both adopt cross sequence semantic information to modulate features in the CSM and ISM stage. In both evaluations, DFSC performs favorably compared with DFSC-all. Class-level semantic modulation in the later stage will makes the tracker confused about the information from different UAVs. As a result, instance-level semantic modulation is necessary for the tracker to enhance discrimination power.

**Influence of Ratio.** The  $\alpha$  means the ratio between  $L_{cross}$  and  $L_{same}$  in Eq. 3. As illustrated in the bottom of Tab. VI,  $mSA$  sharply fluctuates if the ratio  $\alpha$  changes from large to small, in which case DFSC becomes similar to normal method at training time.

With the increase of the ratio  $\alpha$ , the performance first increases and then decreases. When the performance reaches the maximum,  $\alpha$  is about 0.25. And if  $\alpha$  becomes smaller or larger than this value, the performance will decline. This phenomenon is because when  $\alpha$  becomes too large, the tracker will unnecessarily focus too much on the cross sequence feature information. It hinders the tracker from learning class-level semantic feature, which reduces the robustness of the tracker. When  $\alpha$  becomes smaller, DFSC will degenerate into the normal training strategy. DFSC does not always perform better with the increase or decrease of  $\alpha$ , which indicates that different proportion of semantic information collocation plays a different role in the training process of the tracker. A moderate ratio ( $\alpha=0.25$ ) can achieve a trade-off between same sequence semantics and cross sequence semantics.

## VI. CONCLUSION

In the community, there is no high-quality Anti-UAV benchmark for capturing real dynamic scenes. In this paper, the first UAV tracking dataset is constructed, named Anti-UAV, which collects over 300 video pairs and annotates more than 580k bounding boxes manually. Along with the dataset, evaluation

protocols, metrics, and baseline trackers are introduced for the task of UAV tracking. Furthermore, a novel approach named dual-flow semantic consistency (DFSC) is proposed for UAVs tracking. DFSC enables the tracker to fully leverage the semantic information across different video sequences, such that tracker’s robustness and discrimination ability can be further improved. Notably, the proposed DFSC does not introduce any additional inference time. In the future, multi-modal with unaligned data for tracking will be further investigated, which has potential to boost the accurateness of trackers.

## REFERENCES

- [1] X. Li, W. Hu, C. Shen, Z. Zhang, A. R. Dick, and A. van den Hengel, “A survey of appearance models in visual object tracking,” *ACM TIST*, 2013.
- [2] A. W. M. Smeulders, D. M. Chu, R. Cucchiara, S. Calderara, A. Dehghan, and M. Shah, “Visual tracking: An experimental survey,” *TPAMI*, 2014.
- [3] A. Yilmaz, O. Javed, and M. Shah, “Object tracking: A survey,” *ACM Computing Surveys*, 2006.
- [4] I. Haritaoglu, D. Harwood, and L. S. Davis, “W4: real-time surveillance of people and their activities,” *TPAMI*, 2000.
- [5] A. Brunetti, D. Buongiorno, G. F. Trotta, and V. Bevilacqua, “Computer vision and deep learning techniques for pedestrian detection and tracking: A survey,” *Neurocomputing*, 2018.
- [6] X. Yu, Y. Gong, N. Jiang, Q. Ye, and Z. Han, “Scale match for tiny person detection,” in *WACV*, 2020.
- [7] C. Robin and S. Lacroix, “Multi-robot target detection and tracking: taxonomy and survey,” *Autonomous Robots*, 2016.
- [8] M. Chang, J. Lambert, P. Sangkloy, J. Singh, S. Bak, A. Hartnett, D. Wang, P. Carr, S. Lucey, D. Ramanan, and J. Hays, “Argoverse: 3d tracking and forecasting with rich maps,” in *CVPR*, 2019.
- [9] W. Luo, B. Yang, and R. Urtasun, “Fast and furious: Real time end-to-end 3d detection, tracking and motion forecasting with a single convolutional net,” in *CVPR*, 2018.
- [10] S. Lin, M. A. Garratt, and A. J. Lambert, “Monocular vision-based real-time target recognition and tracking for autonomously landing an UAV in a cluttered shipboard environment,” *Autonomous Robots*, 2017.
- [11] H. Cheng, L. Lin, Z. Zheng, Y. Guan, and Z. Liu, “An autonomous vision-based target tracking system for rotorcraft unmanned aerial vehicles,” in *IROS*, 2017.
- [12] L. Bertinetto, J. Valmadre, J. F. Henriques, A. Vedaldi, and P. H. S. Torr, “Fully-convolutional siamese networks for object tracking,” in *ECCVW*, 2016.
- [13] B. Li, J. Yan, W. Wu, Z. Zhu, and X. Hu, “High performance visual tracking with siamese region proposal network,” in *CVPR*, 2018.
- [14] B. Li, W. Wu, Q. Wang, F. Zhang, J. Xing, and J. Yan, “Siamrpn++: Evolution of siamese visual tracking with very deep networks,” in *CVPR*, 2019.

- [15] Q. Wang, L. Zhang, L. Bertinetto, W. Hu, and P. H. S. Torr, "Fast online object tracking and segmentation: A unifying approach," in *CVPR*, 2019.
- [16] M. D. *et al.*, "ATOM: accurate tracking by overlap maximization," in *CVPR*, 2019.
- [17] V. Venkataraman, G. Fan, J. P. Havlicek, X. Fan, Y. Zhai, and M. B. Yeary, "Adaptive kalman filtering for histogram-based appearance learning in infrared imagery," *TIP*, 2012.
- [18] A. Berg, J. Ahlberg, and M. Felsberg, "Channel coded distribution field tracking for thermal infrared imagery," in *CVPRW*, 2016.
- [19] N. Wang, W. Zhou, Q. Tian, R. Hong, M. Wang, and H. Li, "Multi-cue correlation filters for robust visual tracking," in *CVPR*, 2018.
- [20] H. Liu and F. Sun, "Fusion tracking in color and infrared images using joint sparse representation," *SCIENCE CHINA Information Sciences*, 2012.
- [21] Y. Wu, J. Lim, and M. Yang, "Online object tracking: A benchmark," in *CVPR*, 2013.
- [22] Y. Wu and J. L. *et al.*, "Object tracking benchmark," *TPAMI*, 2015.
- [23] M. Kristan and R. P. P. *et al.*, "The visual object tracking VOT2014 challenge results," in *ECCVW*, 2014.
- [24] M. Kristan and A. L. *et al.*, "The visual object tracking VOT2017 challenge results," in *ICCVW*, 2017.
- [25] M. Kristan and A. B. *et al.*, "The seventh visual object tracking VOT2019 challenge results," in *ICCVW*, 2019.
- [26] P. Liang, E. Blasch, and H. Ling, "Encoding color information for visual tracking: Algorithms and benchmark," *TIP*, 2015.
- [27] A. Li, M. Lin, Y. Wu, M. Yang, and S. Yan, "NUS-PRO: A new visual tracking challenge," *TPAMI*, 2016.
- [28] A. Moudgil and V. Gandhi, "Long-term visual object tracking benchmark," in *ACCV*, 2018.
- [29] J. Valmadre, L. Bertinetto, J. F. Henriques, R. Tao, A. Vedaldi, A. W. M. Smeulders, P. H. S. Torr, and E. Gavves, "Long-term tracking in the wild: A benchmark," in *ECCV*, 2018.
- [30] M. Mueller, N. Smith, and B. Ghanem, "A benchmark and simulator for UAV tracking," in *ECCV*, 2016.
- [31] H. K. Galoogahi, A. Fagg, C. Huang, D. Ramanan, and S. Lucey, "Need for speed: A benchmark for higher frame rate object tracking," in *ICCV*, 2017.
- [32] H. Fan, L. Lin, F. Yang, P. Chu, G. Deng, S. Yu, H. Bai, Y. Xu, C. Liao, and H. Ling, "Lasot: A high-quality benchmark for large-scale single object tracking," in *CVPR*, 2019.
- [33] M. Müller, A. Bibi, S. Giancola, S. Al-Subaihi, and B. Ghanem, "Trackingnet: A large-scale dataset and benchmark for object tracking in the wild," in *ECCV*, 2018.
- [34] L. Huang, X. Zhao, and K. Huang, "Got-10k: A large high-diversity benchmark for generic object tracking in the wild," *CoRR*, vol. abs/1810.11981, 2018.
- [35] J. W. Davis and M. A. Keck, "A two-stage template approach to person detection in thermal imagery," in *WACV/MOTION*, 2005.
- [36] J. Portmann, S. Lynen, M. Chli, and R. Siegwart, "People detection and tracking from aerial thermal views," in *ICRA*, 2014.
- [37] Z. Wu, N. W. Fuller, D. H. Theriault, and M. Betke, "A thermal infrared video benchmark for visual analysis," in *CVPRW*, 2014.
- [38] R. Miezianko, "Ieee otcbvs ws series bench," <http://vcipl-okstate.org/pbvs/bench/>, accessed March 4, 2018.
- [39] M. Felsberg, A. Berg, G. Häger, J. Ahlberg, M. Kristan, J. Matas, A. Leonardis, L. Cehovin, G. Fernández, T. Vojtír, G. Nebehay, and R. P. Pflugfelder, "The thermal infrared visual object tracking VOT-TIR2015 challenge results," in *ICCVW*, 2015.
- [40] M. Felsberg, M. Kristan, and J. M. *et al.*, "The thermal infrared visual object tracking VOT-TIR2016 challenge results," in *ECCV*, 2016.
- [41] Q. Liu, Z. He, X. Li, and Y. Zheng, "PTB-TIR: A thermal infrared pedestrian tracking benchmark," *TMM*, 2020.
- [42] Q. Liu, X. Li, Z. He, C. Li, J. Li, Z. Zhou, D. Yuan, J. Li, K. Yang, N. Fan, and F. Zheng, "LSOTB-TIR: A large-scale high-diversity thermal infrared object tracking benchmark," in *ACM MM*, 2020.
- [43] J. W. Davis and V. Sharma, "Background-subtraction using contour-based fusion of thermal and visible imagery," *CVIU*, 2007.
- [44] A. Torabi, G. Massé, and G. Bilodeau, "An iterative integrated framework for thermal-visible image registration, sensor fusion, and people tracking for video surveillance applications," *CVIU*, 2012.
- [45] C. Li, H. Cheng, S. Hu, X. Liu, J. Tang, and L. Lin, "Learning collaborative sparse representation for grayscale-thermal tracking," *TIP*, 2016.
- [46] C. Li, N. Zhao, Y. Lu, C. Zhu, and J. Tang, "Weighted sparse representation regularized graph learning for RGB-T object tracking," in *ACM MM*, 2017.
- [47] C. Li, X. Liang, Y. Lu, N. Zhao, and J. Tang, "RGB-T object tracking: Benchmark and baseline," *PR*, 2019.
- [48] E. Real, J. Shlens, S. Mazzocchi, X. Pan, and V. Vanhoucke, "Youtube-boundingboxes: A large high-precision human-annotated data set for object detection in video," in *CVPR*, 2017.
- [49] D. S. Bolme, J. R. Beveridge, B. A. Draper, and Y. M. Lui, "Visual object tracking using adaptive correlation filters," in *CVPR*, 2010.
- [50] J. F. Henriques, R. Caseiro, P. Martins, and J. P. Batista, "Exploiting the circulant structure of tracking-by-detection with kernels," in *ECCV*, 2012.
- [51] L. Bertinetto, J. Valmadre, S. Golodetz, O. Miksik, and P. H. S. Torr, "Staple: Complementary learners for real-time tracking," in *CVPR*, 2016.
- [52] Z. Han, P. Wang, and Q. Ye, "Adaptive discriminative deep correlation filter for visual object tracking," *TCSVT*, 2020.
- [53] M. Danelljan, F. S. Khan, M. Felsberg, and J. van de Weijer, "Adaptive color attributes for real-time visual tracking," in *CVPR*, 2014.
- [54] Z. Han, J. Jiao, B. Zhang, Q. Ye, and J. Liu, "Visual object tracking via sample-based adaptive sparse repre-

- sentation (adasr),” *PR*, 2011.
- [55] J. F. Henriques, R. Caseiro, P. Martins, and J. Batista, “High-speed tracking with kernelized correlation filters,” *TPAMI*, 2015.
- [56] N. Wang and D. Yeung, “Learning a deep compact image representation for visual tracking,” in *NeurIPS*, 2013.
- [57] M. Danelljan, G. Häger, F. S. Khan, and M. Felsberg, “Convolutional features for correlation filter based visual tracking,” in *ICCV*, 2015.
- [58] C. Ma, J. Huang, X. Yang, and M. Yang, “Hierarchical convolutional features for visual tracking,” in *ICCV*, 2015.
- [59] M. Danelljan, A. Robinson, F. S. Khan, and M. Felsberg, “Beyond correlation filters: Learning continuous convolution operators for visual tracking,” in *ECCV*, 2016.
- [60] M. Danelljan, G. Bhat, F. S. Khan, and M. Felsberg, “ECO: efficient convolution operators for tracking,” in *CVPR*, 2017.
- [61] J. Valmadre, L. Bertinetto, J. F. Henriques, A. Vedaldi, and P. H. S. Torr, “End-to-end representation learning for correlation filter based tracking,” in *CVPR*, 2017.
- [62] I. Jung, J. Son, M. Baek, and B. Han, “Real-time mdnet,” in *ECCV*, 2018.
- [63] H. Nam and B. Han, “Learning multi-domain convolutional neural networks for visual tracking,” in *CVPR*, 2016.
- [64] Y. Zha, T. Ku, Y. Li, and P. Zhang, “Deep position-sensitive tracking,” *TMM*, 2020.
- [65] L. Wang, L. Zhang, J. Wang, and Z. Yi, “Memory mechanisms for discriminative visual tracking algorithms with deep neural networks,” *TCDS*, 2020.
- [66] X. Lu, B. Ni, C. Ma, and X. Yang, “Learning transform-aware attentive network for object tracking,” *Neurocomputing*, 2019.
- [67] Q. Liu, X. Lu, Z. He, C. Zhang, and W. Chen, “Deep convolutional neural networks for thermal infrared object tracking,” *KBS*, 2017.
- [68] P. Gao, Y. Ma, K. Song, C. Li, F. Wang, and L. Xiao, “Large margin structured convolution operator for thermal infrared object tracking,” in *ICPR*, 2018.
- [69] Q. Liu, X. Li, Z. He, N. Fan, D. Yuan, and H. Wang, “Learning deep multi-level similarity for thermal infrared object tracking,” *TMM*, 2020.
- [70] M. Li, L. Peng, Y. Chen, S. Huang, F. Qin, and Z. Peng, “Mask sparse representation based on semantic features for thermal infrared target tracking,” *Remote Sensing*, 2019.
- [71] Y. Wu, E. Blasch, G. Chen, L. Bai, and H. Ling, “Multiple source data fusion via sparse representation for robust visual tracking,” in *FUSION*, 2011.
- [72] K. Zhang, Q. Liu, Y. Wu, and M. Yang, “Robust visual tracking via convolutional networks without training,” *TIP*, 2016.
- [73] S. Zhai, P. Shao, X. Liang, and X. Wang, “Fast RGB-T tracking via cross-modal correlation filters,” *Neurocomputing*, 2019.
- [74] G. Wang, C. Luo, Z. Xiong, and W. Zeng, “Spm-tracker: Series-parallel matching for real-time visual object tracking,” in *CVPR*, 2019.
- [75] L. Huang, X. Zhao, and K. Huang, “Globaltrack: A simple and strong baseline for long-term tracking,” in *AAAI*, 2020.
- [76] L. Ke, M. Chang, H. Qi, and S. Lyu, “Multi-scale structure-aware network for human pose estimation,” in *ECCV*, 2018.
- [77] I. Sáráandi, T. Linder, K. O. Arras, and B. Leibe, “Synthetic occlusion augmentation with volumetric heatmaps for the 2018 ECCV posetrack challenge on 3d human pose estimation,” *CoRR*, vol. abs/1809.04987, 2018.
- [78] H. Zhang, M. Cissé, Y. N. Dauphin, and D. Lopez-Paz, “mixup: Beyond empirical risk minimization,” in *ICLR*, 2018.
- [79] S. Yun, D. Han, S. Chun, S. J. Oh, Y. Yoo, and J. Choe, “Cutmix: Regularization strategy to train strong classifiers with localizable features,” in *ICCV*, 2019.
- [80] Z. Zhu, Q. Wang, B. Li, W. Wu, J. Yan, and W. Hu, “Distractor-aware siamese networks for visual object tracking,” in *ECCV*, 2018.
- [81] H. Possegger, T. Mauthner, and H. Bischof, “In defense of color-based model-free tracking,” in *CVPR*, 2015.
- [82] M. Mueller, N. Smith, and B. Ghanem, “Context-aware correlation filter tracking,” in *CVPR*, 2017.
- [83] F. Li, C. Tian, W. Zuo, L. Zhang, and M. Yang, “Learning spatial-temporal regularized correlation filters for visual tracking,” in *CVPR*, 2018.
- [84] Y. Li, J. Zhu, S. C. H. Hoi, W. Song, Z. Wang, and H. Liu, “Robust estimation of similarity transformation for visual object tracking,” in *AAAI*, 2019.
- [85] M. Danelljan, G. Häger, F. S. Khan, and M. Felsberg, “Accurate scale estimation for robust visual tracking,” in *BMVC*, 2014.
- [86] A. Lukezic, T. Vojir, L. C. Zajc, J. Matas, and M. Kristan, “Discriminative correlation filter with channel and spatial reliability,” in *CVPR*, 2017.
- [87] H. K. Galoogahi, A. Fagg, and S. Lucey, “Learning background-aware correlation filters for visual tracking,” in *ICCV*, 2017.
- [88] Z. Zhang, H. Peng, J. Fu, B. Li, and W. Hu, “Ocean: Object-aware anchor-free tracking,” in *ECCV*, 2020.
- [89] M. Tang, B. Yu, F. Zhang, and J. Wang, “High-speed tracking with multi-kernel correlation filters,” in *CVPR*, 2018.
- [90] Z. Zhang and H. Peng, “Deeper and wider siamese networks for real-time visual tracking,” in *CVPR*, 2019.
- [91] Z. Chen, B. Zhong, G. Li, S. Zhang, and R. Ji, “Siamese box adaptive network for visual tracking,” in *CVPR*, 2020.
- [92] D. Guo, J. Wang, Y. Cui, Z. Wang, and S. Chen, “Siamcar: Siamese fully convolutional classification and regression for visual tracking,” in *CVPR*, 2020.
- [93] G. Bhat, M. Danelljan, L. V. Gool, and R. Timofte, “Know your surroundings: Exploiting scene information for object tracking,” in *ECCV*, 2020.
- [94] G. Bhat, M. Danelljan, and L. V. G. *et al.*, “Learning discriminative model prediction for tracking,” in *ICCV*, 2019.



- [95] K. Dai, Y. Zhang, D. Wang, J. Li, H. Lu, and X. Yang, “High-performance long-term tracking with meta-updater,” in *CVPR*, 2020.
- [96] B. Yan, H. Zhao, D. Wang, H. Lu, and X. Yang, “‘skimming-perusal’ tracking: A framework for real-time and robust long-term tracking,” in *ICCV*, 2019.
- [97] M. Danelljan, L. V. Gool, and R. Timofte, “Probabilistic regression for visual tracking,” in *CVPR*, 2020.
- [98] P. Voigtlaender, J. Luiten, P. H. S. Torr, and B. Leibe, “Siam R-CNN: visual tracking by re-detection,” in *CVPR*, 2020.
- [99] T. Lin, M. Maire, S. J. Belongie, J. Hays, P. Perona, D. Ramanan, P. Dollár, and C. L. Zitnick, “Microsoft COCO: common objects in context,” in *ECCV*, 2014.



**Nan Jiang** received the B.E. degree in communication engineering from Xi’an Jiaotong University, China, in 2018. He is currently pursuing the M.S. degree in computer science with University of Chinese Academy of Sciences. His research interests include machine learning and computer vision.



**Kuiran Wang** received the B.E. degree in computer science and technology from Central South University, China, in 2018. He is currently pursuing the M.S. degree in electronic and communication engineering with University of Chinese Academy of Sciences. His research interests include machine learning and computer vision.



**Xiaoke Peng** received the B.E. degree in communication engineering from Sun Yat-sen University, China, in 2019. She is currently pursuing the M.S. degree in electronic and communication engineering with University of Chinese Academy of Sciences. Her research interests include machine learning and computer vision.



**Xuehui Yu** received the B.E. degree in software engineering from Tianjin University, China, in 2017. He is currently pursuing the Ph.D. degree in signal and information processing with University of Chinese Academy of Sciences. His research interests include machine learning and computer vision.



**Qiang Wang** received the B.S. degree from the University of Science and Technology Beijing, Beijing, China, in 2015, and the Ph.D. degree from the University of Chinese Academy of Sciences (UCAS) in 2020. His research interests include visual tracking, autonomous vehicles, and service robots.

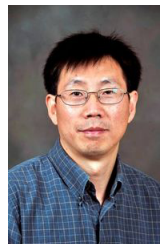


**Junliang Xing** received his dual B.S. degrees in computer science and mathematics from Xi’an Jiaotong University, Shanxi, China, in 2007, and the Ph.D. degree in computer science from Tsinghua University, Beijing, China, in 2012. He is currently a Professor with the National Laboratory of Pattern Recognition, Institute of Automation, Chinese Academy of Sciences, Beijing, China. Dr. Xing was the recipient of Google Ph.D. Fellowship 2011, the Excellent Student Scholarships at Xi’an Jiaotong University from 2004 to 2007 and at Tsinghua University from 2009 to 2011. He has published more than 100 papers on international journals and conferences. His current research interests mainly focus on computer vision problems related to faces and humans.



**Guorong Li** received her B.S. degree in technology of computer application from Renmin University of China, in 2006 and Ph.D. degree in technology of computer application from the Graduate University of the Chinese Academy of Sciences in 2012.

Now, she is an associate professor at the University of Chinese Academy of Sciences. Her research interests include object tracking, video analysis, pattern recognition, and cross-media analysis.



**Guodong Guo** received the B.E. degree in automation from Tsinghua University, Beijing, China, the Ph.D. degree in computer science from University of Wisconsin, Madison, WI, USA. He is currently the Deputy Head of the Institute of Deep Learning, Baidu Research, and also an Associate Professor with the Department of Computer Science and Electrical Engineering, West Virginia University (WVU), USA. In the past, he visited and worked in several places, including INRIA, Sophia Antipolis, France; Ritsumeikan University, Kyoto, Japan; and

Microsoft Research, Beijing, China; He authored a book, “Face, Expression, and Iris Recognition Using Learning-based Approaches” (2008), co-edited two books, “Support Vector Machines Applications” (2014) and “Mobile Biometrics” (2017), co-authored a book, “Multi-Modal Face Presentation Attack Detection” (2020), and published above 100 technical papers. His research interests include computer vision, biometrics, machine learning, and multimedia. He received the North Carolina State Award for Excellence in Innovation in 2008, Outstanding Researcher (2017-2018, 2013-2014) at CEMR, WVU, and New Researcher of the Year (2010-2011) at CEMR, WVU. He was selected the “People’s Hero of the Week” by BSJB under Minority Media and Telecommunications Council (MMTC) in 2013. Two of his papers were selected as “The Best of FG’13” and “The Best of FG’15”, respectively.



**Jian Zhao** received the Bachelors degree from Beihang University in 2012, the Masters degree from National University of Defense Technology in 2014, and the Ph.D. degree from National University of Singapore in 2019. He is currently an Assistant Professor with Institute of North Electronic Equipment, Beijing, China. His main research interests include deep learning, pattern recognition, computer vision and multimedia analysis. He has published over 40 cutting-edge papers. He has received “2021-2023 Beijing Young Talent Support Project” from Beijing

Association for Science and Technology in 2020. He has won the Lee Hwee Kuan Award (Gold Award) on PREMIA 2019, the Best Student Paper Award on ACM MM 2018, and the top-3 awards several times on world-wide competitions. He is the EAC of VALSE, and the committee member of CSIGBVD. He has served as the invited reviewer of NSFC, T-PAMI, IJCV, T-MM, T-IFS, T-CSVT, Neurocomputing, T-CDS, CSSP, JVCI, NeurIPS (one of the top 30% highest-scoring reviewers of NeurIPS 2018), CVPR, ICCV, ACM MM, AAAI, ICLR, ICML, ACCV, UAI.



**Zhenjun Han** received the B.S. degree in software engineering from Tianjin University, Tianjin, China, in 2006 and the M.S. and Ph.D. degrees from University of Chinese Academy of Sciences, Beijing, China, in 2009 and 2012, respectively. Since 2013, he has been an Associate Professor with the School of Electronic, Electrical, and Communication Engineering, University of Chinese Academy of Sciences. His research interests include object tracking and detection.